

Article

Mechanism and kinetics of propane dehydrogenation and cracking over Ga/H-MFI prepared via vapor-phase exchange of H-MFI with GaCl₃

Neelay Phadke, Erum Mansoor, Matthieu Bondil, Martin Head-Gordon, and Alexis T. Bell

J. Am. Chem. Soc., **Just Accepted Manuscript** • DOI: 10.1021/jacs.8b11443 • Publication Date (Web): 26 Dec 2018

Downloaded from <http://pubs.acs.org> on December 27, 2018

Just Accepted

“Just Accepted” manuscripts have been peer-reviewed and accepted for publication. They are posted online prior to technical editing, formatting for publication and author proofing. The American Chemical Society provides “Just Accepted” as a service to the research community to expedite the dissemination of scientific material as soon as possible after acceptance. “Just Accepted” manuscripts appear in full in PDF format accompanied by an HTML abstract. “Just Accepted” manuscripts have been fully peer reviewed, but should not be considered the official version of record. They are citable by the Digital Object Identifier (DOI®). “Just Accepted” is an optional service offered to authors. Therefore, the “Just Accepted” Web site may not include all articles that will be published in the journal. After a manuscript is technically edited and formatted, it will be removed from the “Just Accepted” Web site and published as an ASAP article. Note that technical editing may introduce minor changes to the manuscript text and/or graphics which could affect content, and all legal disclaimers and ethical guidelines that apply to the journal pertain. ACS cannot be held responsible for errors or consequences arising from the use of information contained in these “Just Accepted” manuscripts.

1
2
3 **Mechanism and kinetics of propane dehydrogenation and cracking**
4 **over Ga/H-MFI prepared via vapor-phase exchange of H-MFI with**
5 **GaCl₃**
6
7
8
9

10
11 Neelay M. Phadke^{1‡}

12 Erum Mansoor^{1‡}

13 Matthieu Bondil²

14 Martin Head-Gordon³

15 Alexis T. Bell^{1*}
16
17
18
19
20
21
22
23

24 ¹Department of Chemical and Biomolecular Engineering, University of California, Berkeley, CA
25 94720, USA
26

27 ²Ecole Polytechnique Federale de Lausanne, Lausanne, Switzerland CH-1015
28

29 ³Department of Chemistry, University of California, Berkeley, CA 94720, USA
30
31
32
33

34 Submitted to the Journal of the American Chemical Society

35
36 October 19th, 2018
37
38
39

40
41 ‡ Contributed equally to this work.
42

43 *To whom correspondence should be addressed: alexbell@berkeley.edu
44
45
46
47
48
49
50
51
52
53
54
55
56
57
58
59
60

Abstract

In this study, the mechanism and kinetics of C₃H₈ dehydrogenation and cracking are examined over Ga/H-MFI catalysts prepared via vapor-phase exchange of H-MFI with GaCl₃. The present study demonstrates that [GaH]²⁺ cations are the active centers for C₃H₈ dehydrogenation and cracking, independent of the Ga/Al ratio. For identical reaction conditions, [GaH]²⁺ cations in Ga/H-MFI exhibit a turnover frequency for C₃H₈ dehydrogenation that is two orders of magnitude higher and for C₃H₈ cracking is one order of magnitude higher than the corresponding turnover frequencies over H-MFI. C₃H₈ dehydrogenation and cracking exhibit first-order kinetics with respect to C₃H₈ over H-MFI but both reactions exhibit first-order kinetics over Ga/H-MFI only at very low C₃H₈ partial pressures and zero-order kinetics at higher C₃H₈ partial pressures. H₂ inhibits both reactions over Ga/H-MFI. It is also found that the ratio of the rates of dehydrogenation to cracking over Ga/H-MFI is independent of C₃H₈ and H₂ partial pressures but weakly dependent on temperature. Measured activation enthalpies together with theoretical analysis are consistent with a mechanism in which both the dehydrogenation and cracking of C₃H₈ proceed over Ga/H-MFI via reversible, heterolytic dissociation of C₃H₈ at [GaH]²⁺ sites to form [C₃H₇-GaH]⁺-H⁺ cation pairs. The rate-determining step for dehydrogenation is the β-hydride elimination of C₃H₆ and H₂ from the C₃H₇ fragment. The rate-determining step for cracking is C-C bond attack of the same propyl fragment by the proximal Brønsted acid O-H group. H₂ inhibits both dehydrogenation and cracking over Ga/H-MFI via reaction with [GaH]²⁺ cations to form [GaH₂]⁺-H⁺ cation pairs.

Key words: Propane, dehydrogenation, cracking, Ga/H-MFI, theory

1. Introduction

The increasing availability of large shale gas reserves in the US and across the world, has stimulated interest in finding routes for the catalytic conversion of the condensable components of shale gas components, principally ethane and propane, to alkenes and aromatics via dehydrogenation and dehydrocyclization, respectively.¹⁻⁵ Commercially implemented processes⁶ include the Oleflex and Catofin processes for dehydrogenation which utilize alumina-supported

1
2
3 catalysts and also the Cyclar and Aroforming Processes which use metal-modified zeolite catalysts
4 for dehydroaromatization. Gallium-exchanged H-MFI zeolite (Ga/H-MFI) has been shown to be
5 particularly effective for catalyzing dehydroaromatization reactions.^{5,7-11} For example, the
6 reaction of C₃H₈ over Ga/H-MFI produces higher selectivities to alkenes and aromatics than those
7 observed over unmodified H-MFI.^{10,12} This has led to a renewed interest in studying the structure
8 and catalytic role of Ga species in Ga/H-MFI, as active sites for light alkane conversion.¹³⁻²²

9
10
11
12
13
14
15
16
17
18 The chemical structure and catalytic function of Ga cations in Ga/H-MFI have been
19 examined both experimentally and theoretically.²³ These studies suggest that in the oxidized or
20 reduced state, the following types of species may exist in Ga/H-MFI: [GaO]⁺, [Ga₂O₂]⁺,
21 [Ga(OH)]²⁺, [Ga(OH)₂]⁺, [GaH₂]⁺, [GaH]²⁺, Ga⁺ and GaO_x clusters.^{9,24-32} It should be noted that
22 with the exception of Ga⁺, the oxidation state of Ga in all of the other proposed structures is +3.
23
24
25
26
27
28
29
30
31
32
33
34
35
36
37
38
39
40
41
42
43
44
45
46
47
48
49
50
51
52
53
54
55
56
57
58
59
60
Earlier studies of light alkane dehydrogenation on Ga/H-MFI have reported that oxygen-ligated
species, such as monomeric [GaO]⁺ or dimeric [Ga₂O₂]²⁺ cations are more active than reduced
Ga⁺ cations.^{26,29-31} However, contemporaneous studies as well as more recent ones have suggested
that Ga⁺ cations are the active centers for alkane dehydrogenation.^{9,10,15,28,29,33,34} A variant of this
idea has also been recently proposed, namely that Ga⁺ cations in proximity to Brønsted acid O-H
groups catalyze C₃H₈ dehydrogenation via oxidative addition of H⁺ to Ga⁺ to form a highly Lewis
acidic [GaH]²⁺ species in which the Ga³⁺ center has an oxidation state of +3.²² The role of [GaH]²⁺
cations as the active center for alkane dehydrogenation has also been supported by theoretical
studies. These studies show that divalent [GaH]²⁺ cations, located at proximate cation-exchange
sites in Ga/H-MFI are more active for light alkane dehydrogenation than monovalent [GaH₂]⁺
cations or Ga⁺ cations.^{22,32,35,36}

1
2
3 While a number of authors have proposed that Ga^+ cations are active for the
4 dehydrogenation of light alkanes,^{9,10,15,28,29,33,34,37} the presence of Ga^+ cations in H_2 -reduced Ga/H-
5 MFI has been disputed. Recent work by Getsoian et al. has called into question the interpretation
6 of XANES evidence for Ga^+ cations.¹⁸ These authors note that the decreases in the Ga K-edge
7 XANES edge energy of Ga/H-MFI upon reduction, previously ascribed to formation of Ga^+ ,^{9,10}
8 can be ascribed, instead, to the formation of Ga-alkyl or GaH_x species, in which Ga has a formal
9 oxidation state of +3.¹⁸ Theoretical studies have also shown that the activation barrier for the
10 formation of Ga^+ species in Ga/H-MFI is considerably higher than that for the formation of GaH_x
11 species in which the Ga center has a formal oxidation state of +3.^{36,38}
12
13
14
15
16
17
18
19
20
21
22
23

24 A further issue complicating the identification of the catalytically active species in Ga/H-
25 MFI is the synthetic protocol typically employed for the preparation of Ga/H-MFI – incipient
26 wetness impregnation of H-MFI with an aqueous solution of a Ga salt, most notably $\text{Ga}(\text{NO}_3)_3$.³⁹
27 Steric and electronic constraints associated with large aqueous Ga^{3+} complexes result in a slow
28 diffusion of Ga into the MFI micropores leading to low levels of ion-exchange and the deposition
29 of GaO_x agglomerates at the external surfaces of the zeolite crystal.^{23,40} Upon contact with H_2 or
30 alkane reactants at reaction temperatures (> 700 K), ion-exchange has been reported to occur via
31 conversion of GaO_x into volatile Ga_2O monomers.⁹ However, the resulting materials have been
32 reported to still contain detectable concentrations of GaO_x .⁴⁰ The presence of neutral GaO_x
33 together with ion-exchanged Ga^{3+} cations in Ga/H-MFI prepared via the conventional protocol has
34 precluded accurate determination of the active Ga structures and their catalytic role in light alkane
35 dehydrogenation and dehydroaromatization.
36
37
38
39
40
41
42
43
44
45
46
47
48
49
50
51

52 We report here a detailed study of the mechanism and kinetics of C_3H_8 dehydrogenation
53 and cracking over Ga/H-MFI with Ga/Al ratios of 0.05 to 0.3. These catalysts were prepared by
54
55
56
57

1
2
3 reaction of the Brønsted acid O-H groups in H-MFI with GaCl₃ vapor under anhydrous conditions
4
5 at elevated temperature, followed by stoichiometric removal of Ga-bound Cl by H₂ reduction,
6
7 resulting in the formation of GaH_x (x = 1, 2) structures. Detailed characterization of these samples
8
9 shows that for Ga/Al ratios below 0.3, and upon reduction under anhydrous conditions, all of the
10
11 Ga is present as isolated [GaH]²⁺ cations or as [GaH₂]⁺-H⁺ cation pairs; neutral GaO_x agglomerates
12
13 are undetectable in these samples.⁴¹ Both types of cationic species are associated with proximate
14
15 cation-exchange sites associated with NNN (Next-nearest neighboring i.e separated by a -O-Si-O
16
17 linkage) or NNNN (Next, next-nearest neighboring i.e separated by a -O-Si-O-Si-O linkage) pairs
18
19 of framework Al atoms. Our investigations show that C₃H₈ dehydrogenation over these samples
20
21 of Ga/H-MFI occurs primarily over [GaH]²⁺ cations, independent of the Ga/Al ratio, at a rate (per
22
23 Al_{tot} atom) that is two orders of magnitude higher than that occurring over isolated Brønsted acid
24
25 O-H groups located in H-MFI, under identical reaction conditions. The rate of C₃H₈ cracking to
26
27 CH₄ and C₂H₄ over Ga/H-MFI is an order of magnitude higher than that over H-MFI and also
28
29 occurs over [GaH]²⁺ sites. While both cracking and dehydrogenation exhibit first-order
30
31 dependences on C₃H₈ partial pressure over H-MFI, the rates of both reactions exhibit a Langmuir-
32
33 Hinshelwood dependence on C₃H₈ over Ga/H-MFI and are inhibited by H₂. Over H-MFI, both the
34
35 dehydrogenation and cracking of C₃H₈ occur over Brønsted acid O-H groups. In the case of Ga/H-
36
37 MFI, examination of alternative reaction pathways via experiment and theory suggests that both
38
39 reactions occur preferentially on [GaH]²⁺ sites via mechanisms involving C₃H₈ derived [C₃H₇-
40
41 GaH]⁺ intermediates. Inhibition of both reactions by H₂ is proposed to occur via the formation of
42
43 [GaH₂]⁺-H⁺ cation pairs.
44
45
46
47
48
49
50
51
52
53
54
55
56
57
58
59
60

2. Experimental and theoretical methods

2.1 Preparation of H-MFI and Ga/H-MFI

NH₄⁺-MFI (Zeolyst, CBV 3024E) was converted to the H-form by heating it at 2 K min⁻¹ to 773 K in dry synthetic air (Praxair, ultrazero, 100 cm³ min⁻¹) and then holding it at this temperature for 4 h. The Si/Al_{tot} ratio of this sample is 16.5 ± 1.0, as determined by ICP-OES (Galbraith Laboratories, Knoxville, TN). Ga/H-MFI samples with varying Ga/Al ratios (0.05-0.5) were prepared via anhydrous exchange of dehydrated H-MFI with GaCl₃ vapor, using a protocol developed by our group. A detailed discussion of the preparation and characterization of these samples is given in Ref. 41.

2.2 Reaction rate measurements

Reaction rates for C₃H₈ conversion over H-MFI and Ga/H-MFI were measured using a tubular quartz plug flow reactor. Catalyst samples (~5-12 mg) were placed over a quartz wool plug, fitted inside the reactor (30.5 cm in length and 0.64 cm in outer diameter). Catalyst charges less than 8 mg were diluted with SiO₂ (Silia Flash 150A). The reactor was heated by means of a ceramic cylindrical furnace. The temperature of the catalyst bed was measured by a K-type thermocouple (Omega) connected to a temperature controller (Omega), to maintain the catalyst temperature. Gases were metered into the reactor by means of mass flow controllers (MFC) (Porter), which were calibrated using a bubble flow meter. Prior to making rate measurements, samples were heated at 2 K min⁻¹ from ambient temperatures to 773 K under flowing dry synthetic air (Praxair, ultrazero, 100 cm³ min⁻¹) and held at this temperature for 1 h. This oxidative pre-treatment was used for H-MFI and Ga/H-MFI. Reductive pre-treatment of Ga/H-MFI was carried out by purging the system with He following the oxidative treatment at 773 K and then switching

1
2
3 the reactor feed to a gas mixture of 2.5% H₂ diluted in He (Praxair, CSG, 100 cm³ min⁻¹). Samples
4
5 were held at this temperature under H₂ for 1 h.
6
7

8
9 Following either oxidative or reductive pre-treatments, samples were exposed to flowing
10 mixtures of C₃H₈/He prepared by diluting a 20% C₃H₈/He stream (Praxair, CSG) with He (Praxair,
11 UHP) in order to generate C₃H₈ partial pressures ranging from 0.25-11 kPa. Experiments involving
12
13 co-fed H₂ were conducted by adding H₂ to the feed flow. For this purpose, a 2.5 % H₂/He stream
14
15 (Praxair, CSG) was mixed with the C₃H₈/He stream in order to obtain H₂ partial pressures ranging
16
17 from 0.25-1.5 kPa. The total pressure of the system was maintained at 101.32 kPa. He, H₂ and dry
18
19 synthetic air were further purified by passing these gases through purifiers (VICI) in order to
20
21 remove trace amounts of H₂O or hydrocarbons. Gas flow rates were varied (100-350 cm³ min⁻¹) in
22
23 order to measure catalyst activity at different space times (defined as mol Al_{tot}*s/mol C₃H₈) for a
24
25 given C₃H₈/H₂/He feed composition. A heated line connected to the outlet of the reactor was used
26
27 to transfer reactants and reaction products to a gas chromatograph (GC) (Agilent 7890A). The
28
29 reactor effluent present in a sample loop was injected periodically into the GC. Reactants and
30
31 products were separated by a capillary column (Agilent 1909IP-Q02, 25 m X 350 μm X 10 μm)
32
33 and were detected by means of a flame ionization detector (FID). FID Response factors for
34
35 hydrocarbons species were obtained by diluting a pre-calibrated gas mixture containing CH₄, C₂H₆
36
37 , C₂H₄, C₃H₈, C₃H₆, C₄H₁₀, C₄H₈ with He to attain different concentrations of the component
38
39 hydrocarbons. The response factors for C₆H₆ and C₇H₈ were determined by directly injecting
40
41 known amounts of liquid C₆H₆ and C₇H₈ into the GC injector.
42
43
44
45
46
47
48
49

50
51 The conversion of C₃H₈ over H-MFI and Ga/H-MFI was measured at differential
52 conversions (< 9 % C₃H₈ conversion) at temperatures between 718 K and 753 K. Plots of
53
54 conversion vs space time were linear for each feed composition combination and extrapolated to
55
56
57

1
2
3 zero conversion at zero space time, consistent with reactor operation under a differential
4 conversion regime. Selectivities were defined on both a C-basis and C₃H₈ basis. C₃H₈
5
6 dehydrogenation rates were determined from C₃H₆ concentrations, while C₃H₈ cracking rates were
7
8 determined from the concentrations of either CH₄ or C₂H₄ cracking products. When product
9
10 selectivities were extrapolated to zero space time, cracking rates derived from CH₄ concentrations
11
12 were similar to those determined from C₂H₄ concentrations. The C₃H₈ partial pressures (0.25 – 11
13
14 kPa) and H₂ partial pressures (0.25-1.5 kPa) were varied in a non-systematic fashion in order to
15
16 examine the effects of reactant and product pressures on measured rates. For each combination of
17
18 C₃H₈/H₂ partial pressures, rates were measured at four different space times. By this means, rates
19
20 could be extrapolated linearly to 0 space time. Moreover, after measurements had been made at
21
22 each C₃H₈/H₂ pressure combination, rates were measured at 0.9 kPa C₃H₈/He at a space time of 9
23
24 mol Al*s /mol C₃H₈ in order to assess and correct for catalyst deactivation. Catalyst deactivation
25
26 did not exceed 5% in typical experiments. Activation enthalpies and entropies were extracted by
27
28 relations (equations S24-S26) derived from transition state theory.⁴² For the application of these
29
30 equations, rate coefficients (per Al_{tot} atom) were normalized by the fraction of [GaH]²⁺ cations
31
32 per Al_{tot} atom determined via NH₃-TPD measurements (details described in S..⁴¹
33
34
35
36
37
38
39
40
41
42
43

44 **2.3 Theoretical methods.**

45
46
47 The hybrid Quantum Mechanics/Molecular Mechanics (QM/MM)^{43,44} approach used in
48
49 this work takes into account the impact of long-range dispersive interactions and the polarization
50
51 of the active site by the electrostatic field associated with the zeolite lattice, both of which are
52
53 critical to capturing reaction energetics accurately.⁴⁵ A T437 atom cluster is used to represent the
54
55
56
57
58
59
60

1
2
3 zeolite framework surrounding the active site. The QM region consists of either a T5 or a T9 cluster
4
5 representing the part of the zeolite associated with the extra-framework cation (H^+ or $[Ga(H)_n]^{(3-$
6
7 $n)^+}$) and any adsorbed species. The MM region is modeled with an improved parametrization;⁴⁶
8
9 framework Si and O atoms are fixed at their crystallographic positions. The framework Al atom
10
11 associated with extraframework Ga cationic species is taken to be at the T12 site. This T site is
12
13 located in the channel intersections of MFI.⁴⁷ Both the activities of Brønsted acid O-H groups and
14
15 Lewis acidic $[GaH]^{2+}$ cations are investigated. As shown previously, only a small difference (2.6
16
17 kcal/mol) was found in the calculated barriers for C_2H_4 methylation over H-MFI calculated for
18
19 both T5 and T20 clusters,⁴⁸ which suggests that our QM/MM approach is not influenced
20
21 significantly by the size of the QM region used. An illustration of the model used for the $[GaH]^{2+}$
22
23 cation in this study is shown in Figure S.5 and is discussed in more detail in earlier work.³⁶
24
25
26
27

28
29 Stationary and saddle point searches were conducted at the ω B97X-D/6-31G** level of
30
31 theory using the default optimization procedure available in QChem.⁴⁹ The reported activation
32
33 energies were computed using the ω B97X-D functional⁵⁰ with the triple- ζ , split-valence Pople
34
35 basis set, with diffuse and polarization functions 6-311++G(3df,3pd). While recent developments
36
37 in DFT have led to functionals with statistically improved accuracy^{51,52} relative to ω B97X-D, we
38
39 note that the QM/MM parameters were developed specifically for that functional. Enthalpy and
40
41 entropy calculations were performed using the Quasi Rigid Rotor Harmonic Oscillator (RRHO)
42
43 approximation. We have used this approach successfully in previous studies to obtain activation
44
45 enthalpies and entropies for n - C_4H_{10} reactions in H-MFI, yielding good agreement with
46
47 experimental results.⁵³ For each mechanism examined, we determined the value of ΔG^\ddagger from the
48
49 respective free energy surface using energetic span model proposed by Kozuch and Shaik.⁵⁴⁻⁵⁷
50
51
52
53
54
55
56
57
58
59
60

3. Results and Discussion

3.1 C₃H₈ conversion over H-MFI via monomolecular dehydrogenation and cracking

For times-on-stream < 100 min, the rate of C₃H₈ dehydrogenation over H-MFI decreased monotonically, before approaching a steady-state (see Figure S.1). However, the rate of C₃H₈ cracking did not change appreciably with time on stream. These trends are similar to those reported for n-C₄H₁₀ dehydrogenation and cracking over H-MFI.⁵⁸ The authors of that study proposed that the high initial rate of C₃H₈ dehydrogenation is attributable to Lewis acidic, extra-framework Al (EFAl) sites that deactivate during the first 100 min of reaction. All steady-state rates were therefore measured over H-MFI, after the deactivation period (~100 min).

The steady-state product molar ratios of H₂/C₃H₆ and C₂H₄/CH₄ during C₃H₈ conversion over H-MFI were close to unity, consistent with previous studies of C₃H₈ dehydrogenation and cracking over H-MFI.⁵⁸⁻⁶⁰ As seen in Figure 1a and 1b, the rates of both dehydrogenation and cracking are first-order in C₃H₈ partial pressure, also in agreement with previous reports for monomolecular dehydrogenation and cracking catalyzed by Brønsted acid O-H groups at low alkane partial pressures.^{61,62}

Apparent first-order rate coefficients were measured at different temperatures (see Figure S.2.) and these data were used to determine apparent activation enthalpies (ΔH_{app}) for C₃H₈ dehydrogenation and cracking. The experimentally measured apparent activation enthalpies for C₃H₈ dehydrogenation and cracking were found to be 40.6 ± 2.9 kcal/mol and 34.6 ± 3.8 kcal/mol, respectively (reported uncertainties reflect 95% confidence intervals). Both estimates are consistent with previous reported estimates of activation energies for C₃H₈ monomolecular dehydrogenation (22.7- 47.8 kcal/mol) and monomolecular cracking (35.1 -37.7 kcal/mol) over H-

MFI.^{59,60,63,64} We also obtained theoretical estimates of apparent activation enthalpies for these reactions occurring over isolated Brønsted acid O-H groups in H-MFI via QM/MM calculations. Apparent activation enthalpies estimated in this manner are 47.5 kcal/mol for methyl-C₃H₈ dehydrogenation, 35.3 kcal/mol for methylene-C₃H₈ dehydrogenation and 33.3 kcal/mol for C₃H₈ cracking. The activation enthalpy for methylene-C₃H₈ dehydrogenation is expected to be significantly lower than that for methyl C₃H₈- dehydrogenation, due to the higher stability of the secondary carbenium ion in the late dehydrogenation transition state of the former pathway relative to the primary carbenium formed in the late dehydrogenation transition state of the latter pathway. Consistent with this interpretation, our experimental measurements are in good agreement with theoretical predictions for methylene dehydrogenation and cracking. The transition state structures and free energy surfaces for these mechanisms are presented in Figure S.13-14 of the S.I.

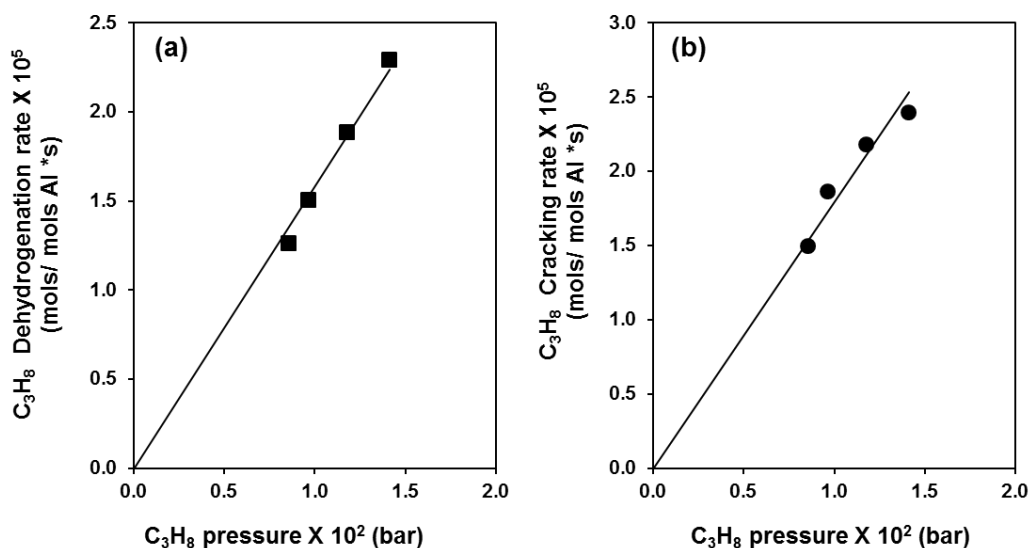


Figure 1: (a) Dependence of C₃H₈ dehydrogenation rates (per Al_{tot} atom) over H-MFI on C₃H₈ partial pressure at 733 K. (b) Dependence of C₃H₈ cracking rates (per Al_{tot} atom) over H-MFI at 733 K on C₃H₈ partial pressure at 733 K. Solid lines indicate regressed first-order slopes.

3.2 C₃H₈ conversion over oxidized and H₂-reduced Ga/H-MFI

Figure 2a shows the rates of C₃H₈ consumption at 733 K over Ga/H-MFI (Ga/Al = 0.2) under differential reaction conditions (C₃H₈ conversion < 9%). Following oxidative pre-treatment of Ga/H-MFI (at 773 K in flowing dry air for 1h), the rate of C₃H₈ consumption increases monotonically with time-on-stream for ~ 300 min before approaching a steady-state (red curve, Figure 2a). This slow induction period suggests that Ga species undergo structural transformation before reaching their steady-state structure. Also shown in Figure 2a, is the rate of C₃H₈ consumption as a function of time-on-stream for Ga/H-MFI (Ga/Al = 0.2) reduced in 2.5% H₂/He for 1 h at 823 K prior to measurements of the reaction rate (blue curve, Figure 2a). In this case, no induction period is observed and the steady-state rate of C₃H₈ consumption is nearly identical to that measured for the oxidized sample.

Product selectivities (expressed as the fraction of converted carbon in each product) are shown as a function of time-on-stream in Figure 2b, for oxidized and H₂-reduced Ga/H-MFI. Throughout the duration of the experiment, the dominant product is C₃H₆, produced via C₃H₈ dehydrogenation. The selectivity to C₃H₆ does not change with time-on-stream or catalyst pre-treatment. The same is true for the selectivity to CH₄. For the oxidized sample, the selectivities to C₂H₄ and aromatics increase slightly as a function of time on stream, but approach the same values as that observed for the reduced sample. While C₂H₄ is formed as a primary product via cracking of C₃H₈, space time studies (see Section S.3) indicate that C₂H₄ is also produced via secondary pathways at higher conversions. These experiments also show that aromatics are produced exclusively via secondary pathways which become increasingly prevalent at higher conversion. Therefore the concentrations of both C₂H₄ and aromatics are expected to increase as the rate of C₃H₈ consumption for oxidized Ga/H-MFI increases with time-on-stream. Thus, the product

1
2
3 selectivity trends seen in Figure 2b suggest that similar active sites catalyze C₃H₈ dehydrogenation
4 and cracking and that the concentration of these active sites increases with time-on-stream for
5 oxidized Ga/H-MFI or upon pre-reduction of the catalyst in H₂.
6
7
8
9

10
11 The results presented in Figure 2, together with our earlier characterization work,⁴¹ suggest
12 that [GaH]²⁺ cations and/or [GaH₂]⁺-H⁺ cation pairs formed upon H₂ reduction of Ga/H-MFI are
13 the active species for C₃H₈ dehydrogenation and cracking. We propose that during the induction
14 period observed for oxidized Ga/H-MFI, [Ga(OH)]²⁺ cations and [Ga(OH)₂]⁺-H⁺ cation pairs
15 undergo reduction to form [GaH]²⁺ cations and [GaH₂]⁺-H⁺ cation pairs.
16
17
18
19
20
21
22

23
24 As shown in Section S.3, secondary reactions are prevalent even under conditions of
25 differential conversion. We also show in Figure S.4 and Section 3.4 that the rates of
26 dehydrogenation and cracking over Ga/H-MFI are inhibited by H₂. To eliminate the effects of
27 product inhibition and secondary reactions, all of the steady-state measured reaction rates reported
28 in the balance of this study were extrapolated to zero space time (see Figure S.4).
29
30
31
32
33
34
35
36
37
38
39
40
41
42
43
44
45
46
47
48
49
50
51
52
53
54
55
56
57
58
59
60

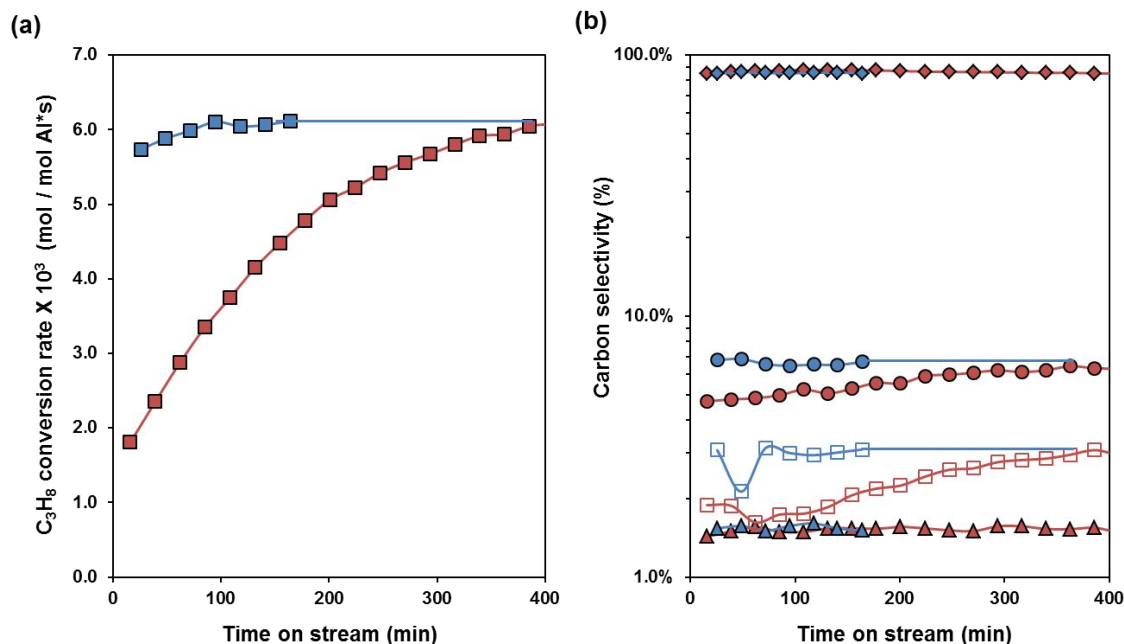


Figure 2: (a) C₃H₈ consumption rates (per Al_{tot} atom) and (b) Percent carbon selectivities for Ga/H-MFI (Ga/Al = 0.2) measured at 733 K with 0.9 kPa C₃H₈/He and $\tau = 9$ (mol Al*s/mol C₃H₈) space time. Blue data points indicates Ga/H-MFI pre-treated in 2.5% H₂/He at 823 K for 1 h prior to reaction, while red data points indicates Ga/H-MFI pre-treated in synthetic dry air at 773 K for 1 h prior to reaction. In Figure 2b, diamonds indicate C₃H₆, circles indicate C₂H₄, open squares indicate aromatics, and triangles indicate CH₄ selectivities.

3.3 Effects of Ga content on the rates of C₃H₈ dehydrogenation and cracking over Ga/H-MFI

Figures 3a-3c and 4a-4c show C₃H₈ dehydrogenation and cracking rates, measured at 733 K and 0.9 kPa C₃H₈/He over H-MFI and Ga/H-MFI, as functions of the Ga/Al ratio. As observed in Figure 3a, the rate of C₃H₈ dehydrogenation (normalized per Al_{tot} atom), increases with Ga content up to a Ga/Al ratio of 0.1 but then reaches a plateau for higher values of Ga/Al ratio. At this plateau, the rate of C₃H₈ dehydrogenation is ~500 times higher than the corresponding rate over H-MFI, suggesting that the reactivity contribution of residual Brønsted acid O-H acid groups in Ga/H-MFI is negligible.

1
2
3 The rate of C₃H₈ dehydrogenation over Ga/H-MFI can also be normalized per Ga atom by
4 dividing the rate per Al_{tot} by the Ga/Al_{tot} ratio. The rate of C₃H₈ dehydrogenation normalized this
5 way, shown in Figure 3b, decreases monotonically as the Ga/Al ratio increases from 0.05 to 0.5,
6 suggesting that the most active Ga species exist at the lowest Ga/Al ratios. As discussed earlier,
7 our characterization of H₂-reduced Ga/H-MFI samples used in the present study shows that for
8 Ga/Al ≤ 0.3, the dominant Ga species present are [GaH]²⁺ cations and [GaH₂]⁺-H⁺ cations pairs,
9 and that 100% of the Ga is present as [GaH]²⁺ cations for Ga/Al = 0.1.⁴¹ Moreover, the theoretical
10 calculations supporting this work show that the formation of [GaH]²⁺ cations is thermodynamically
11 favored at NNN cation-exchange sites associated with pairs of framework Al atoms ≤ 5 Å apart.
12
13
14
15
16
17
18
19
20
21
22
23
24 ⁴¹ Increasing the Ga/Al ratio results in the formation of [GaH₂]⁺-H⁺ cation pairs at NNN and
25 NNNN cation-exchange sites associated with framework Al-Al interatomic distances > 5 Å apart.⁴¹
26
27
28
29
30
31
32
33
34
35
36
37
38
39
40
41
42
43
44
45
46
47
48
49
50
51
52
53
54
55
56
57
58
59
60

Our recent theoretical calculation have shown that [GaH]²⁺ cations are more active for C₃H₈ dehydrogenation than [GaH₂]⁺-H⁺ cation pairs.³⁶ We also note in Figure 3a that the rate of dehydrogenation (per Al_{tot}) over the Ga/Al = 0.5 sample, which contains neutral GaO_x oligomeric species, in addition to cation-exchanged Ga³⁺ species, is identical to the corresponding rate (per Al_{tot}) over samples with lower Ga content. This suggests that neutral GaO_x species are much less active for C₃H₈ conversion in comparison to cation-exchanged Ga³⁺ species.

Based on the foregoing discussion, we normalized the rate of C₃H₈ dehydrogenation by the density of [GaH]²⁺ cations per Al_{tot} measured for each Ga/Al ratio, measured via NH₃-TPD (see S.I. S.6 for the method by which the density of [GaH]²⁺ cations was estimated).⁴¹ Figure 3c shows that the rate of C₃H₈ dehydrogenation normalized this way is nearly independent of the Ga/Al ratio. It should be noted that the rate of C₃H₈ dehydrogenation per [GaH]²⁺ for the Ga/Al = 0.05 sample is about 20% higher than that for the remaining samples, which may reflect small

differences between the actual fraction of $[\text{GaH}]^{2+}$ cations present in the $\text{Ga}/\text{Al} = 0.05$ sample and our estimate. We therefore conclude that the rate of C_3H_8 dehydrogenation is approximately independent of the Ga/Al ratio. This finding supports the prediction that $[\text{GaH}]^{2+}$ cations are the most active species for C_3H_8 dehydrogenation and that $[\text{GaH}_2]^+-\text{H}^+$ cation pairs, which constitute an increasing fraction of the Ga content in Ga/H-MFI samples with $\text{Ga}/\text{Al} > 0.1$, do not to contribute appreciably to the measured rate.^{36, 41}

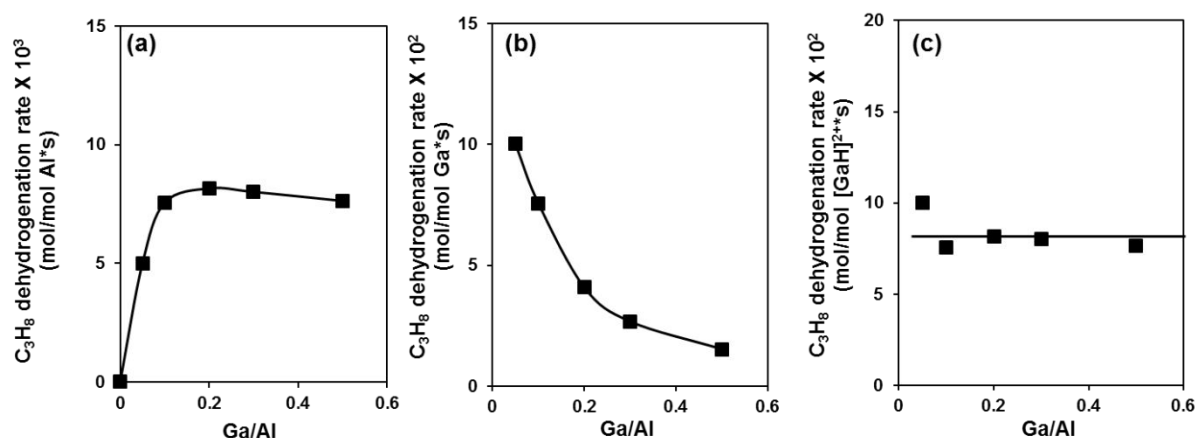


Figure 3: C_3H_8 dehydrogenation rates, measured at 0.9kPa $\text{C}_3\text{H}_8/\text{He}$ and 733 K as a function of Ga/Al ratio, with rates over Ga/H-MFI extrapolated to zero space time. Conversions $< 9\%$ (a) Rates normalized per Al_{tot} atom (b) Rates normalized per Ga atom (c) Rates normalized per $[\text{GaH}]^{2+}$ estimated via NH_3 -TPD.⁴¹ Solid lines are guides for the eye.

Figures 4a-4c show C_3H_8 cracking rates over H-MFI and Ga/H-MFI, also measured at 0.9 kPa $\text{C}_3\text{H}_8/\text{He}$ and 733 K. Here again, measured cracking rates over Ga/H-MFI were extrapolated to zero space time. The rate of C_3H_8 cracking normalized per Al_{tot} atom (Figure 4a) shows a trend similar to that of the rate of C_3H_8 dehydrogenation, increasing with Ga content up to a Ga/Al ratio of 0.1, and then reaching a plateau for higher Ga/Al ratios. At similar conditions, the maximum rate of C_3H_8 cracking over Ga/H-MFI (per Al_{tot} atom) is about 20 times higher than that over H-MFI.

1
2
3 It is notable that an enhancement in the rate of alkane cracking over Co, Zn and Ga-
4 exchanged zeolites, relative to the corresponding H-forms of these zeolites, has been reported
5 previously.^{15,37,65-67} Alkane cracking over these metal-exchanged zeolites has been attributed to
6 H₂-assisted alkane hydrogenolysis catalyzed by Ga sites^{15,66,67} or to protolytic cracking of C-C
7 bonds by residual Brønsted acid O-H groups,^{33,37} the acid strength of which may be enhanced by
8 proximity to exchanged metal cations.^{68,69} Therefore, both of these possibilities need to be
9 considered as possible causes for the higher rate of C₃H₈ cracking over Ga/H-MFI.

10
11
12
13
14
15
16
17
18
19
20 H₂-assisted hydrogenolysis of C₃H₈ would be expected to result in higher cracking rates
21 with increasing H₂ concentration at higher space times (or C₃H₈ conversion) or upon co-feeding
22 H₂. On the contrary, we find that the rate of C₃H₈ cracking decreases with an increase in C₃H₈
23 conversion and is inhibited by co-feeding H₂ (see Figure S.4 and Section 3.4). These results suggest
24 that hydrogenolysis does not contribute to C₃H₈ cracking over Ga/H-MFI. An alternative
25 explanation is that the higher rate of C₃H₈ cracking over Ga/H-MFI compared to H-MFI could be
26 attributable to an increase in the acid strength of Brønsted acid O-H groups that are proximate to
27 metal cations (here, [GaH₂]⁺ cations).^{68,69} This phenomenon should lead to an increase in the rate
28 of C₃H₈ cracking with an increase in the concentration of [GaH₂]⁺-H⁺ cation pairs as the Ga/Al
29 ratio increases. However, cracking rates normalized per Al_{tot} atom do not increase with Ga content
30 beyond a Ga/Al ratio of 0.1 (Figure 4a), while cracking rates normalized per Ga atom (Figure 4b)
31 decrease monotonically with increasing Ga content. It is also notable, that when normalized by the
32 estimated density of [GaH]²⁺ cations per Al_{tot} (see S.I. S.6 for the method by which the density of
33 [GaH]²⁺ cations was estimated), the rate of C₃H₈ cracking is independent of the Ga/Al ratio, as can
34 be seen in Figure 4c. Taken together, these data suggest that [GaH]²⁺ cations rather than H₂-
35 assisted hydrogenolysis by Ga sites or protolytic cracking by residual Brønsted acid O-H groups
36
37
38
39
40
41
42
43
44
45
46
47
48
49
50
51
52
53
54
55
56
57
58
59
60

proximate to $[\text{GaH}_2]^+$ cations, are responsible for the observed enhancements in cracking rates over Ga/H-MFI. Further evidence in support of this conclusion is given below.

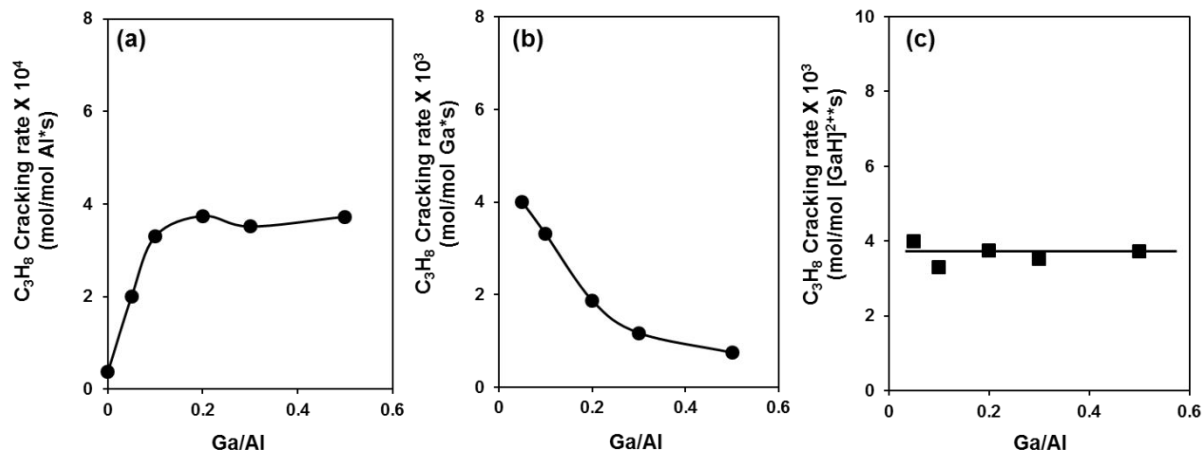


Figure 4: C_3H_8 cracking rates over H-MFI and Ga/H-MFI, measured at 0.9 kPa $\text{C}_3\text{H}_8/\text{He}$ and 733 K. Rates over Ga/H-MFI were extrapolated to 0 space time. Conversions $< 9\%$ (a) Rates normalized per Al_{tot} atom (b) Rates normalized per Ga atom (c) Rates normalized per $[\text{GaH}]^{2+}$ estimated via NH_3 -TPD measurements. Dotted lines are guides for the eye.

3.4 Effects of C_3H_8 and H_2 partial pressures on the rates of C_3H_8 dehydrogenation and cracking over Ga/H-MFI

The rates of C_3H_8 dehydrogenation and cracking (per Al_{tot} atom and extrapolated to zero space time) are shown in Figure 5a and 5b respectively as functions of C_3H_8 partial pressure and temperature. At all three temperatures (718, 733, 753 K), the rates of C_3H_8 dehydrogenation and cracking increase monotonically with C_3H_8 partial pressure at low partial pressures but become independent with respect to C_3H_8 partial pressure at higher pressures. Figure 5c shows the dependence of the ratio of the rate of dehydrogenation to cracking (D/C), as a function of the C_3H_8 partial pressure. For a given temperature, no discernable trend is evident in the D/C ratio as a function of C_3H_8 partial pressure, suggesting that the D/C ratio is approximately independent of the surface coverage of adsorbed C_3H_8 . This observed trend suggests that both dehydrogenation

1
2
3 and cracking proceed over identical active sites in Ga/H-MFI and via a common C₃H₈-derived
4 surface intermediate. However, the D/C ratio does exhibit a weak dependence on temperature,
5 increasing from approximately 19.1 at 753K to approximately 24.6 at 718 K. An increase in the
6 value of this ratio with a decrease in temperature is consistent with the activation energy for
7 cracking being higher than that for dehydrogenation.
8
9
10
11
12
13

14
15 As shown in Figure S.4, H₂ inhibits the rate of C₃H₈ dehydrogenation and cracking over
16 Ga/H-MFI. The dependence of these rates on H₂ partial pressure at 733 K is shown in Figures 6a-
17 6c. While the rates of C₃H₈ dehydrogenation and cracking decrease with an increase in H₂ partial
18 pressure, inhibition of these rates is more severe at lower partial pressures of C₃H₈ and relatively
19 weaker at high partial pressures of C₃H₈. Apparent reaction orders of H₂ for dehydrogenation and
20 cracking at each C₃H₈ partial pressure measured at 733 K are provided in Table S1 of the
21 supplementary information. These effects of H₂ partial pressure are consistent with H₂ competing
22 with C₃H₈ for adsorption on the active sites that catalyze both reactions. As shown in Figure 6c,
23 the D/C ratio is independent of H₂ and C₃H₈ partial pressures, suggesting that H₂ inhibits both
24 dehydrogenation and cracking in a similar fashion and further supports the idea that
25 dehydrogenation and cracking occur on the same active sites.
26
27
28
29
30
31
32
33
34
35
36
37
38
39
40

41 The observed effects of C₃H₈ and H₂ partial pressures on the rates of C₃H₈ dehydrogenation
42 and cracking are consistent with rate laws of the form given by Eqns. 1 and 2, respectively. Since
43 the D/C ratio is nearly independent of the C₃H₈ and H₂ partial pressures, the denominator terms in
44 Eqns. 1 and 2 are taken to be the same.
45
46
47
48
49
50

$$\frac{\text{Dehydrogenation rate}}{A_{\text{tot}}} = \frac{\alpha_d[\text{C}_3\text{H}_8]}{1 + \beta[\text{C}_3\text{H}_8] + \gamma[\text{H}_2]} \quad (1)$$

51
52
53
54
55
56
57
58
59
60

$$\frac{\text{Cracking rate}}{Al_{\text{tot}}} = \frac{\alpha_c [C_3H_8]}{1 + \beta [C_3H_8] + \gamma [H_2]} \quad (2)$$

Here, α_d (dehydrogenation), α_c (cracking), β and γ are parameters related to the kinetics and thermodynamics of the elementary steps involved in C_3H_8 dehydrogenation and cracking.

Nonlinear regression of the data shown in Figures 5a-c and 6a-c to Eqns. 1 and 2, respectively, results in a satisfactory fit, represented by the solid lines in these figures. Values of α_d , α_c , β , and γ at 733 K are presented in Table 1. At very low partial pressures of C_3H_8 and in the absence of co-fed H_2 , Eqns. 1 and 2 and, the data in Figures 5 and 6 indicate that the rates of dehydrogenation and cracking exhibit a first-order dependence on C_3H_8 partial pressure. The parameters, α_d and α_c therefore reflect apparent first-order rate coefficients (k_{app}) for dehydrogenation and cracking with units of mol/mol $Al_{\text{tot}} \cdot s \cdot \text{bar}$. At very high partial pressures of C_3H_8 and in the absence of H_2 , the rates of dehydrogenation and cracking are independent of C_3H_8 partial pressure, as seen from the data in Figure 5. In this case, the ratios α_d/β and α_c/β correspond to the zero-order rate coefficients (k_{int}) with units of mol/mol $Al_{\text{tot}} \cdot s$. Therefore, for consistency the parameters β and γ must have units of bar^{-1} and hence correspond to the adsorption coefficients (K_{ads}) for C_3H_8 and H_2 , respectively. Further interpretation of the parameters α , β , and γ are discussed below in the context of our examination of possible mechanisms for C_3H_8 dehydrogenation and cracking over Ga/H-MFI.

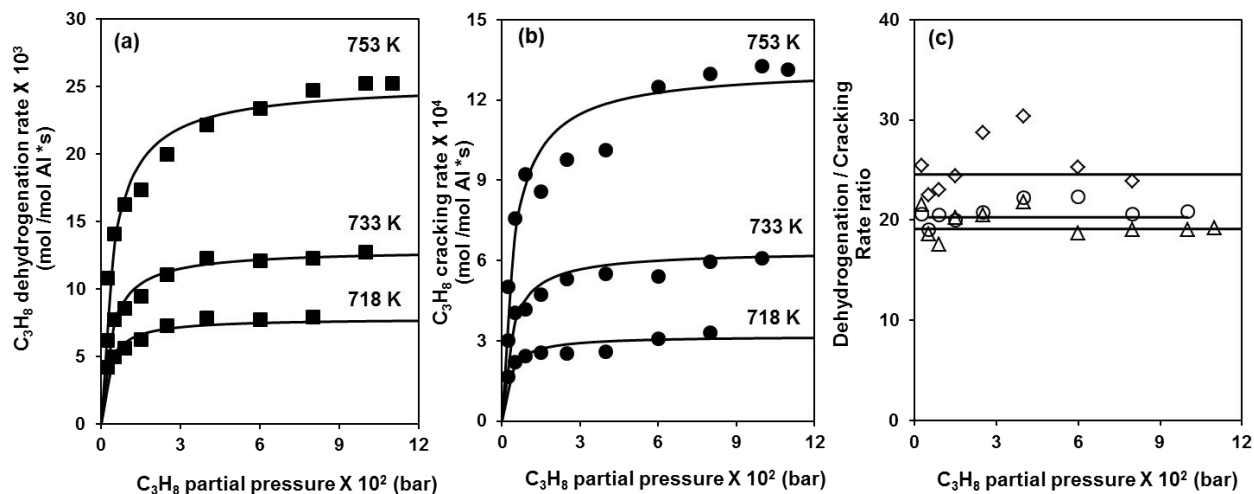


Figure 5: (a) Dependence of the rates of C₃H₈ dehydrogenation and (b) C₃H₈ cracking, and (c) the ratio of the rates of dehydrogenation to cracking over Ga/H-MFI (Ga/Al = 0.2) measured at 718, 733 and 753 K, on the C₃H₈ partial pressure. In Figure 5c, triangles, circles, and diamonds indicate the ratios of rates at 718 K, 733 K, and 753 K, respectively. All rates were extrapolated to zero space time. Solid lines show regressed fits of Eqns. 1 and 2 to the data.

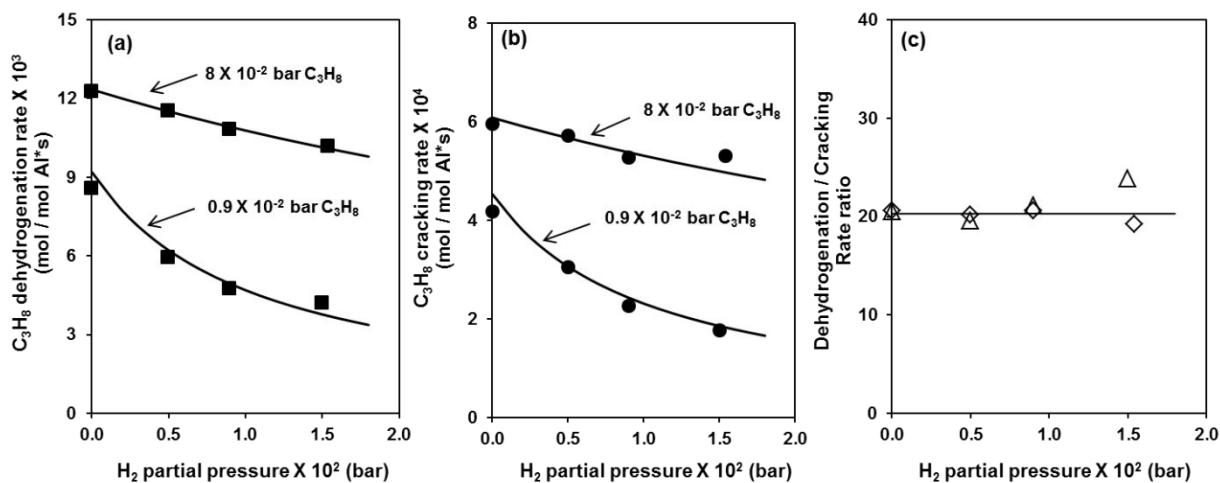


Figure 6: Effects of H₂ partial pressure on the rates of (a) C₃H₈ dehydrogenation and (b) C₃H₈ cracking, and (c) the ratio of the rates of dehydrogenation to cracking (D/C) measured at 733 K. All rates were extrapolated to zero space time. In Figure 6c, open triangles indicate the D/C ratios measured at 0.9 × 10⁻² bar C₃H₈ and open diamonds indicate the D/C rate ratios measured at 8 × 10⁻² bar C₃H₈. Solid lines in Figures 6a-c show regressed fits to Eqns. 1 and 2 to the data.

Table 1: Values of parameters obtained by non-linear least squares regression of Eqns. 1 and 2 to the rates of C₃H₈ dehydrogenation and cracking measured at 733 K, shown in Figures 5 and 6. The parameters β and γ were common to both dehydrogenation and cracking in Eqns. 1 and 2, respectively.

	α (k_{app}) (mol/mol Al _{tot} *s*bar)	β (K_{adsC3}) (bar ⁻¹)	γ (K_{adsH2}) (bar ⁻¹)	$\alpha/\beta(k_{int})$ (mol/mol Al _{tot} *s)
Dehydrogenation	3.6	2.8 X 10 ²	3.3 X 10 ²	1.3 X 10 ⁻²
Cracking	1.8 X 10 ⁻¹	2.8 X 10 ²	3.3 X 10 ²	6.4 X 10 ⁻⁴

3.5 Mechanisms for C₃H₈ dehydrogenation and cracking over [GaH]²⁺ sites

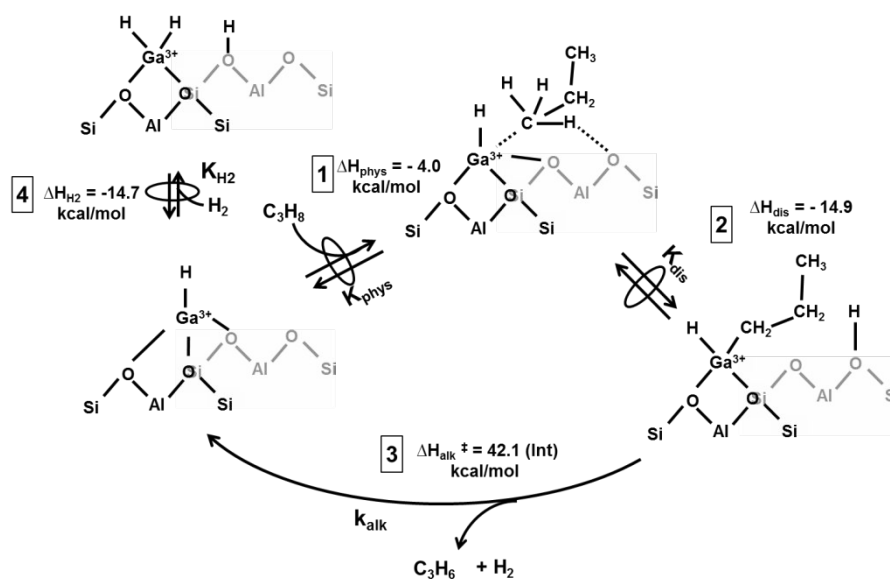
Based on the insight gained in Section 3.3 and 3.4 regarding the role of [GaH]²⁺ cations in catalyzing C₃H₈ dehydrogenation, we can propose two distinct mechanisms by which C₃H₈ undergoes dehydrogenation over [GaH]²⁺ sites- a) an alkyl mechanism b) a carbenium mechanism.³⁶ In addition, we propose an alkyl mechanism to describe the role of [GaH]²⁺ cations in the cracking of C₃H₈. The elementary steps for the alkyl and carbenium mechanisms for C₃H₈ dehydrogenation and the alkyl mechanism for C₃H₈ cracking over [GaH]²⁺ sites, are described in Schemes 1, 2 and 3, respectively. Detailed Gibbs free energy and enthalpy reaction coordinate diagrams are also provided for each of the reaction mechanisms in Figures S.6-S.9. The elementary steps presented in Schemes 1-3 can be used to derive rate equations that describe the kinetic behavior predicted by each of the mechanisms, presented here as Equation 3 for alkyl mediated dehydrogenation, Equation 4 for carbenium mediated dehydrogenation and Equation 5 for alkyl mediated cracking. The assumptions and methods used to derive these equations are described in detail in Section S.4.

$$\frac{\text{Dehydrogenation rate}}{[\text{GaH}]^{2+}} = \frac{k_{alk}K_{dis}K_{phys}[C_3H_8]}{1 + (K_{dis}K_{phys})[C_3H_8] + K_{H_2}[H_2]} \quad (3)$$

$$\frac{\text{Dehydrogenation rate}}{[\text{GaH}]^{2+}} = \frac{k_{\text{carb}}K_{\text{phys}}[\text{C}_3\text{H}_8]}{1 + K_{\text{H}_2}[\text{H}_2]} \quad (4)$$

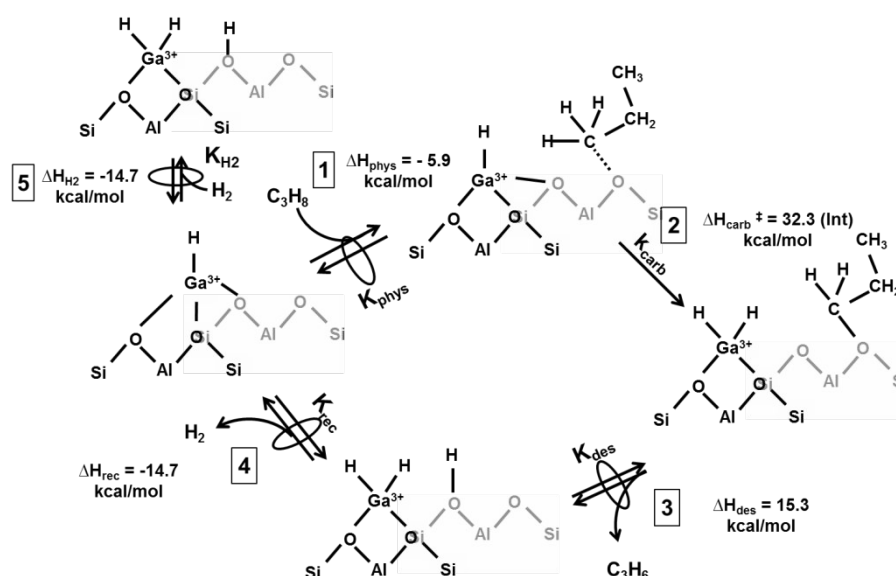
$$\frac{\text{Cracking rate}}{[\text{GaH}]^{2+}} = \frac{k_{\text{crack}}K_{\text{dis}}K_{\text{phys}}[\text{C}_3\text{H}_8]}{1 + (K_{\text{dis}}K_{\text{phys}})[\text{C}_3\text{H}_8] + K_{\text{H}_2}[\text{H}_2]} \quad (5)$$

In Equations 3 and 4, k_{alk} and k_{carb} are the rate coefficients for the rate-determining, β -hydride elimination step in the alkyl dehydrogenation sequence (Step 3 in Scheme 1) and the rate-determining carbenium C-H activation step in the carbenium dehydrogenation sequence (Step 2 in Scheme 2), respectively. In Equation 5 k_{crack} is the rate coefficient for the rate-determining C-C bond attack step in the alkyl cracking mechanism (Step 3 in Scheme 3). K_{dis} is the equilibrium constant for heterolytic dissociation of C_3H_8 to form $[\text{C}_3\text{H}_7\text{-GaH}]^+\text{-H}^+$ cation pairs and K_{phys} is the adsorption constant for C_3H_8 physisorption at $[\text{GaH}]^{2+}$ sites. K_{H_2} is the equilibrium constant for dissociative adsorption of H_2 at $[\text{GaH}]^{2+}$ sites to form $[\text{GaH}_2]^+\text{-H}^+$ cation pairs.

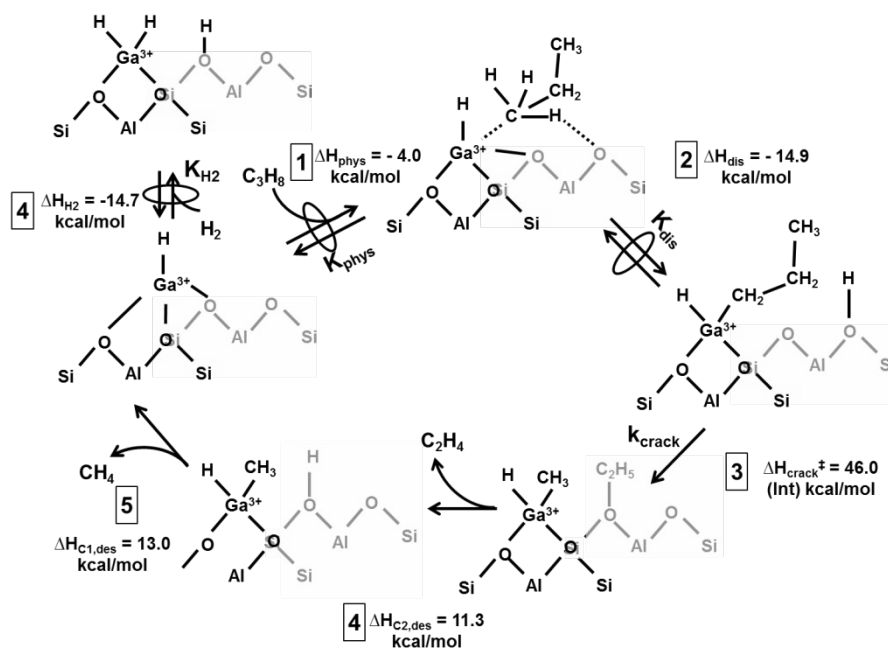


Scheme 1: Alkyl mechanism for activation and dehydrogenation of C_3H_8 over $[\text{GaH}]^{2+}$ sites to C_3H_6 and H_2 . Enthalpies (adsorption, reaction and activation) for each step are shown here with respect to the enthalpy of the initial structure in the step. For each structure, framework atoms that are faded reflect cation-exchange sites that are behind the image plane for non-faded cation-

exchange sites. Cations coordinated to the faded cation-exchange sites are also behind the image plane but have not been faded for visual purposes



Scheme 2: Carbenium mechanism for the activation and conversion of C_3H_8 to C_3H_6 and H_2 over $[GaH]^{2+}$ sites. Enthalpies (adsorption, reaction and activation) for each step are shown here with respect the enthalpy of the initial structure in the step. For each structure, framework atoms that are faded reflect cation-exchange sites that are behind the image plane for non-faded cation-exchange sites. Cations coordinated to the faded cation-exchange sites are also behind the image plane but have not been faded for visual purposes



Scheme 3: Cracking of C_3H_8 over $[\text{GaH}]^{2+}$ sites by the alkyl mechanism. Enthalpies (adsorption, reaction and activation) for each step are shown here with respect the enthalpy of the initial structure in the step. For each structure, framework atoms that are faded reflect cation-exchange sites that are behind the image plane for non-faded cation-exchange sites. Cations coordinated to the faded cation-exchange sites are also behind the image plane but have not been faded for visual purposes

As seen in Schemes 1-3, alkyl mediated pathways for dehydrogenation and cracking over $[\text{GaH}]^{2+}$ require dissociative adsorption of C_3H_8 over $[\text{GaH}]^{2+}$ to produce $[\text{C}_3\text{H}_7\text{-GaH}]^+\text{-H}^+$ cation pairs, prior to the rate-determining step. On the other hand, the carbenium mediated dehydrogenation pathway proceeds via rate-determining C-H activation of C_3H_8 species, physisorbed at $[\text{GaH}]^{2+}$. In all three cases, inhibition of rates is predicted to occur via dissociative adsorption of H_2 at $[\text{GaH}]^{2+}$ to form $[\text{GaH}_2]^+\text{-H}^+$ cation pairs. These observations, together with an inspection of rate equations (3-5) show that only the alkyl-mediated mechanisms predict a first order dependence of dehydrogenation and cracking rates on C_3H_8 at low C_3H_8 partial pressures and an inhibition of these rates by C_3H_8 at high C_3H_8 partial pressures via the saturation of $[\text{GaH}]^{2+}$

1
2
3 sites by strongly-bound $[\text{C}_3\text{H}_7\text{-GaH}]^+$ species. In the carbenium mechanism, the relatively weak
4 binding of C_3H_8 to $[\text{GaH}]^{2+}$ sites, prior to the rate-determining C-H activation step, would lead to
5 a first-order dependence of the rate of dehydrogenation on the C_3H_8 partial pressure, in the absence
6 of H_2 , as predicted by Equation 4.
7
8
9
10
11
12

13 As seen in Figures 5 and 6, the dependence of the experimentally measured
14 dehydrogenation and cracking rates on C_3H_8 partial pressure is only consistent with the kinetics
15 predicted by the alkyl-mediated mechanisms. Similarly, the D/C rate ratio in Figure 5c and Figure
16 6c is independent of C_3H_8 and H_2 partial pressures. These observations are also consistent with the
17 conclusion that C_3H_8 dehydrogenation and cracking are catalyzed via a common, strongly bound
18 C_3H_8 derived surface intermediate. The alkyl mechanisms for dehydrogenation and cracking also
19 proceed via a common C_3H_8 derived reactive intermediate i.e., $[\text{C}_3\text{H}_7\text{-GaH}]^+\text{-H}^+$ cation pairs.
20
21
22
23
24
25
26
27
28
29

30 A further assessment of the relevant mechanisms involved in C_3H_8 dehydrogenation and
31 cracking over Ga/H-MFI can be obtained by comparing experimentally derived activation and
32 adsorption enthalpies to their values predicted theoretically. Experimental activation and
33 adsorption enthalpies were obtained by measuring the rates of C_3H_8 dehydrogenation and cracking
34 at different temperatures (718-753 K) over the Ga/Al = 0.2 sample and then determining values of
35 the apparent and intrinsic activation enthalpies for both reactions. The methods used for extracting
36 values of these parameters from kinetic data are provided in Section S.5 and plots showing the
37 temperature dependence of rate coefficients and adsorption coefficients are provided in Figures
38 S.10-S.12.
39
40
41
42
43
44
45
46
47
48
49
50

51 Experimental values of the activation and adsorption enthalpies for C_3H_8 dehydrogenation
52 and cracking over Ga/H-MFI (Ga/Al = 0.2) are given in Table 2. Also shown in this table, are the
53
54
55
56
57
58
59
60

1
2
3 apparent and intrinsic activation and adsorption enthalpies predicted from QM/MM calculations
4
5 for the alkyl and carbenium mechanisms for C₃H₈ dehydrogenation and for the alkyl mechanism
6
7 for C₃H₈ cracking, in all three cases over [GaH]²⁺ sites. For C₃H₈ dehydrogenation, the
8
9 experimentally measured apparent activation enthalpy is 19.0 ± 6.0 kcal/mol and the intrinsic
10
11 activation enthalpy is 34.6 ± 1.0 kcal/mol, whereas the adsorption enthalpy for C₃H₈ extracted
12
13 from experimental data is -15.6 ± 5.0 kcal/mol. These estimates of the C₃H₈ adsorption enthalpy
14
15 and the apparent and intrinsic enthalpies are consistent with theoretical predictions for the
16
17 formation of [C₃H₇-GaH]⁺-H⁺ cation pairs upon dissociative C₃H₈ adsorption at [GaH]²⁺ sites (-
18
19 18.9 kcal/mol) and β-hydride elimination of C₃H₆ and H₂ (predicted ΔH_{app} = 23.2 kcal/mol and
20
21 predicted ΔH_{int} = 42.1 kcal/mol). As noted earlier, the carbenium mechanism involves the
22
23 activation of an adsorbed C₃H₈ precursor that is weakly bound to the active site leading to smaller
24
25 differences between the apparent and intrinsic activation enthalpies, than those measured
26
27 experimentally and to a rate expression for C₃H₈ dehydrogenation that is inconsistent with that
28
29 observed experimentally (compare Eqn. 1 with Eqns. 3 and 4).
30
31
32
33
34
35

36 The DFT-predicted value for the dissociative adsorption of C₃H₈ on [GaH]²⁺ is more
37
38 exothermic than that for dissociative adsorption of H₂, a finding that is consistent with the
39
40 experimentally-measured adsorption enthalpies reported in Table 2. However, the value for the
41
42 predicted adsorption enthalpy of H₂ at [GaH]²⁺ sites is lower than that deduced from the analysis
43
44 of the reaction kinetics. A part of this discrepancy may be due to the sensitivity of the predicted
45
46 value to the interatomic distance between framework Al atoms involved in proximate cation-
47
48 exchange sites which host [GaH]²⁺ cations.^{35,36} For the NNN Al atom configurations considered,
49
50 the predicted enthalpy for dissociative adsorption of H₂ on [GaH]²⁺ cations to form [GaH₂]⁺-H⁺
51
52
53
54
55
56
57
58
59
60

cation pairs varies between -5.5 to -15.9 kcal/mol. This range encompasses the experimental H₂ adsorption enthalpy value of -7.4 ± 3.3 kcal/mol shown in Table 2.

Table 2 also shows apparent and intrinsic activation enthalpies for C₃H₈ cracking via the alkyl mechanism over [GaH]²⁺ predicted from theoretical calculations. The experimentally measured apparent activation enthalpy (26.5 ± 0.3 kcal/mol) is in excellent agreement with the theoretically predicted estimate (27.1 kcal/mol). The experimentally measured intrinsic activation enthalpy, 42 ± 4.7 kcal/mol is also in good agreement with the theoretical estimate (44.9 kcal/mol).

Table 2: Apparent and intrinsic activation enthalpies for C₃H₈ dehydrogenation and cracking over Ga/H-MFI (Ga/Al = 0.2), extracted from Figures S11-S13 in the S.I. and enthalpies of dissociative adsorption for C₃H₈ and H₂. Also shown are theoretically predicted activation enthalpies for C₃H₈ dehydrogenation and cracking over [GaH]²⁺ via alkyl and carbenium mechanisms and for the enthalpies of dissociative adsorption for C₃H₈ and H₂. Reported uncertainties reflect 95% confidence intervals.

Enthalpy (kcal/mol)	Dehydrog. Experiment ^a	Alkyl dehydrog. mechanism ^b	Carbenium dehydrog. mechanism ^b	Cracking Experiment ^a	Alkyl cracking mechanism ^b
ΔH_{app}^\ddagger	19.0 ± 6.0	23.2	26.4	26.5 ± 0.3	27.1
ΔH_{int}^\ddagger	34.6 ± 1.0	42.1	32.3	42.0 ± 4.7	46.0
$\Delta H_{ads}(C_3H_8)$	-15.6 ± 5.0	-18.9	-5.9	-15.6 ± 5.0	-18.9
$\Delta H_{ads}(H_2)$	-7.4 ± 3.3	-14.6	-14.6	-7.4 ± 3.3	-14.6

^a From fits of regressed first and zero order rate constants (k_{app} and k_{int}) measured at temperatures ranging from 718 K- 753 K for the Ga/Al = 0.2 sample, to equations 1 and 2. Rate coefficients were obtained via non-linear regression of rate data in Figure 5 and 6 to Equation 1 and 2 and they were normalized to the fraction of [GaH]²⁺ sites, estimated from NH₃-TPD measurements (See S.I, S.6).⁴¹ Apparent and intrinsic activation enthalpies and adsorption enthalpies were obtained via linear regression of rate coefficient data to Equations S24, S25 and S26.

^b Computed using QM/MM methods. See theoretical methods section for more details

1
2
3 The data presented in Table 2 further support the hypothesis that both dehydrogenation and
4 cracking of C₃H₈ over Ga/H-MFI are catalyzed by [GaH]²⁺ sites via a common alkyl-Ga, [C₃H₇-
5 GaH]⁺ surface intermediate. Inhibition of both rates occurs by dissociative adsorption of H₂ at
6 [GaH]²⁺ to form [GaH₂]⁺-H⁺ cation pairs. Consistent with this interpretation, the D/C ratio, shown
7 in Figure 5c and Figure 6c, is independent of C₃H₈ and H₂ surface coverage, but weakly dependent
8 on temperature. Therefore, the selectivity to C₃H₈ dehydrogenation versus cracking over Ga/H-
9 MFI is not governed by the concentrations of C₃H₈, H₂ or residual Brønsted acid O-H groups in
10 Ga/H-MFI, but rather by the difference between the free energy activation barriers for
11 dehydrogenation and cracking over [GaH]²⁺. A higher activation enthalpy for cracking than for
12 dehydrogenation would lead to a decrease in the D/C ratio with an increase in temperature, as
13 observed experimentally in Figure 5c. Indeed, Table 2 indicates that the difference in the measured
14 activation enthalpies (apparent or intrinsic) between cracking and dehydrogenation over Ga/H-
15 MFI, $\Delta\Delta H_{C/D}^{\ddagger}(\text{exp})$ is 7.4 ± 4.8 kcal/mol. Consistent with this finding, our theoretical calculations
16 predict a higher activation enthalpy for alkyl mediated cracking, than for alkyl mediated
17 dehydrogenation ($\Delta\Delta H_{C/D}^{\ddagger}(\text{calc}) = 3.9$ kcal/mol).
18
19
20
21
22
23
24
25
26
27
28
29
30
31
32
33
34
35
36
37

38 We turn next to a comparison of our results with those recently reported by Schreiber et
39 al.³⁷ Ga/H-MFI samples (Si/Al =50) in their work were prepared using conventional incipient
40 wetness impregnation followed by H₂ reduction. Both C₃H₈ dehydrogenation and cracking rates
41 were shown to increase with Ga content up to a Ga/Al ratio of 0.5, with further increases in Ga
42 content leading to lower rates of dehydrogenation and cracking. Similar to our findings, the rate
43 of C₃H₈ dehydrogenation was shown to exhibit a Langmuir-Hinshelwood dependence on C₃H₈
44 partial pressure but the dependence of the rate of dehydrogenation on H₂ partial pressure was not
45 investigated.
46
47
48
49
50
51
52
53
54
55
56
57
58
59
60

1
2
3 Schreiber et al. have proposed that $\text{Ga}^+\text{-H}^+$ cation pairs are responsible for the
4 dehydrogenation of C_3H_8 . This conclusion is based on the observation of a peak at 10,370.2 eV in
5 the XANES spectrum of their sample of H_2 - reduced Ga/H-MFI attributed to Ga^+ cations and to
6 the observation that the rate of dehydrogenation increases with Ga content up to a Ga/Al ratio of
7 0.5.³⁷ Periodic Density Functional Theory (DFT) calculations were then employed to show how
8 $\text{Ga}^+\text{-H}^+$ cation pairs residing at proximate cation-exchange sites associated with NNN pairs of
9 framework Al atoms could catalyze C_3H_8 dehydrogenation. In this scheme, the $\text{Ga}^+\text{-H}^+$ cation pair
10 is first converted into a $[\text{GaH}]^{2+}$ cation via oxidative addition and the latter species is assumed to
11 catalyze the alkyl C–H activation of C_3H_8 to form a $[\text{C}_3\text{H}_7\text{-GaH}]^+\text{-H}^+$ cation pair. This step is then
12 followed by a monomolecular elimination of H_2 from the $[\text{C}_3\text{H}_7\text{-GaH}]^+\text{-H}^+$ cation pair and
13 subsequent release of C_3H_6 to regenerate $\text{Ga}^+\text{-H}^+$ cation pair sites. Both alkyl C-H activation and
14 H_2 elimination steps were reported to be kinetically relevant.

15
16
17
18
19
20
21
22
23
24
25
26
27
28
29
30
31 We have examined several aspects of the mechanism proposed by Schieber et al.³⁷ The
32 first is the ability of $[\text{GaH}]^{2+}$ cations to undergo reductive elimination to form $\text{Ga}^+\text{-H}^+$ cation pairs.
33 We find that the Gibbs free energy for this reaction is -10.4 kcal/mol and that the free energy
34 barrier for the reductive elimination of H^+ from $[\text{GaH}]^{2+}$ to form $\text{Ga}^+\text{-H}^+$ cation pairs is 25.2
35 kcal/mol. This indicates that the formation of $\text{Ga}^+\text{-H}^+$ cation pairs from $[\text{GaH}]^{2+}$ cations is both
36 thermodynamically and kinetically feasible (see Figure S.8). However, the free energy (77.8
37 kcal/mol) and enthalpy (26.3 kcal/mol) activation barriers for the C-H activation step via the
38 mechanism reported by Scheiber et al. on the given $[\text{GaH}]^{2+}$ site, are considerably higher than the
39 corresponding values reported in Scheme 1 and in Figure S7, 40.1 kcal/mol and 2.0 kcal/mol,
40 respectively. We believe that the difference in the energetics reported here and by Scheiber et al.³⁷
41 is a consequence of how $[\text{GaH}]^{2+}$ cations are coordinated with the zeolite framework. In the latter
42
43
44
45
46
47
48
49
50
51
52
53
54
55
56
57
58
59
60

1
2
3 study, $[\text{GaH}]^{2+}$ cations are bound to two framework O atoms, whereas in our work, $[\text{GaH}]^{2+}$ cations
4
5 are bound to three framework O atoms (and one H ligand), thus forming the preferred tetrahedral
6
7 coordination around the Ga^{3+} center.⁷⁰ The three framework O atoms in the first coordination
8
9 sphere of these species withdraw more electron density from the Ga^{3+} center resulting in $[\text{GaH}]^{2+}$
10
11 cations that are more Lewis acidic and therefore more reactive towards alkane C-H activation than
12
13 $[\text{GaH}]^{2+}$ cations that are bound to only two framework O atoms.
14
15

16
17 We have also investigated the free energy landscape for the dehydrogenation pathway over
18
19 Ga^+-H^+ cation pairs proposed by Schreiber et al. Our calculations indicate that the rate-determining
20
21 step for this sequence is the concerted elimination of C_3H_6 and H_2 from $[\text{C}_3\text{H}_7-\text{GaH}]^+-\text{H}^+$ cation
22
23 pairs to reform Ga^+-H^+ cation pairs (see Figure S8). The Gibbs free energy barrier for this rate-
24
25 determining transition state is about 20 kcal/mol higher than that for the rate-determining step in
26
27 the alkyl sequence over $[\text{GaH}]^{2+}$ shown in Scheme 1 (see Figure S7), thereby rendering the former
28
29 pathway less favorable. Thus, while our theoretical calculations predict that the formation of Ga^+-
30
31 H^+ cation pairs from $[\text{GaH}]^{2+}$ cations is thermodynamically and kinetically feasible, these
32
33 calculations also predict that the dehydrogenation of C_3H_8 via processes involving Ga^+-H^+ cation
34
35 pairs would be much less favorable than those involving $[\text{GaH}]^{2+}$ cations. We also show that while
36
37 Ga^+-H^+ cation pairs can activate C_3H_8 to produce $[\text{C}_3\text{H}_7-\text{GaH}]^+-\text{H}^+$ cation pairs, upon C_3H_6
38
39 formation from these species the barrier to form $[\text{GaH}]^{2+}$ cations is much lower than that to
40
41 regenerate Ga^+-H^+ cation pairs (see Figure S15). Therefore, our findings strongly suggest that
42
43 $[\text{GaH}]^{2+}$ cations are the primary active sites responsible for dehydrogenation.
44
45
46
47
48
49
50

51 **4. Conclusions**

52
53 The kinetics of C_3H_8 dehydrogenation and cracking were investigated over Ga/H-MFI, prepared
54
55 with Ga/Al ratios between 0.05 and 0.3, for which all of the Ga is presented as isolated cationic
56
57

1
2
3 species. C_3H_8 conversion occurs over H-MFI via monomolecular dehydrogenation and cracking
4 catalyzed by Brønsted O-H acid groups. C_3H_8 conversion over pre-oxidized Ga/H-MFI undergoes
5 an induction period before reaching a steady-state activity. The induction period is significantly
6 attenuated by pre-reducing the catalysts in H_2 . Notably, the distribution of products formed via
7 C_3H_8 dehydrogenation and cracking are virtually unchanged during the induction period and the
8 steady-state activities of Ga/H-MFI are independent of the initial state of cationic Ga^{3+} species
9 (oxidized or reduced). Reaction rates (expressed per Al_{tot} atom) for C_3H_8 dehydrogenation and
10 cracking over Ga/H-MFI (Ga/Al = 0.2) are ~ 500 and ~ 20 times respectively higher than the
11 corresponding rates over H-MFI at identical conditions. Rates of both reactions, when normalized
12 with respect to the concentration of $[GaH]^{2+}$ cations are found to be independent of the Ga/Al ratio,
13 suggesting that $[GaH]^{2+}$ cations are the catalytically active centers for both reactions. C_3H_8
14 dehydrogenation and cracking rates over Ga/H-MFI are first-order in C_3H_8 at low C_3H_8 partial
15 pressures and are inhibited by C_3H_8 at higher C_3H_8 partial pressures. Both reactions are inhibited
16 by the presence of H_2 . Ratios of the rates of dehydrogenation to cracking (D/C) are, however,
17 independent of the partial pressures of C_3H_8 and H_2 and only dependent upon temperature, again
18 suggesting that both reactions involve the same active center. The observed dependences of
19 reaction rates on the partial pressures of C_3H_8 and H_2 as well as both the apparent and intrinsic
20 activation enthalpies are consistent with theoretical predictions based on a proposed alkyl mediated
21 mechanism for the two reactions. The alkyl mediated mechanism for C_3H_8 dehydrogenation and
22 cracking begins with the reversible, dissociative adsorption of C_3H_8 at $[GaH]^{2+}$ to form $[C_3H_7-$
23 $GaH]^{+}-H^{+}$ cation pairs. Dehydrogenation then proceeds via rate-determining β -hydride elimination
24 from the C_3H_7 fragment to form C_3H_6 and H_2 in a concerted step involving a cyclic transition state.
25 On the other hand, cracking proceeds via rate-determining C-C bond attack of the C_3H_7 fragment
26
27
28
29
30
31
32
33
34
35
36
37
38
39
40
41
42
43
44
45
46
47
48
49
50
51
52
53
54
55
56
57
58
59
60

1
2
3 by the proximal Brønsted acid O-H group, resulting in the formation of $[\text{CH}_3\text{-GaH}]^+$ cations
4
5 proximal to ethoxide species. C_2H_4 and CH_4 are then formed in subsequent steps that are not
6
7 kinetically relevant. Inhibition of both dehydrogenation and cracking by H_2 occurs via dissociative
8
9 adsorption of H_2 at $[\text{GaH}]^{2+}$ cations to produce $[\text{GaH}_2]^+\text{-H}^+$ cation pairs, which are much less active
10
11 for C_3H_8 dehydrogenation and cracking.
12
13
14
15
16
17

18 **Associated content:**

19
20 The Supporting Information for this work is available free of charge on the internet and
21
22 includes details regarding characterization, catalytic rate measurements and theoretical
23
24 calculations.
25
26
27
28
29

30 **Acknowledgements**

31
32 This work was supported by Chevron Energy Technology Company. Computational
33
34 resources were provided by the Molecular Graphics and Computation Facility (supported by NIH
35
36 S100D023532). We would like to thank Christopher Ho for helpful technical discussions. E.M.
37
38 gratefully acknowledges support from the Abu Dhabi National Oil Company in the form of a
39
40 fellowship. M. B. acknowledges support provided to him as a visiting scholar by Prof. Liubov
41
42 Kiwi-Minsker of the Ecole Polytechnique Federale de Lausanne, Lausanne, Switzerland.
43
44
45
46
47
48

49 **References:**

- 50
51 (1) Siirola, Jeffrey, J. The Impact of Shale Gas in the Chemical Industry. *AIChE J.* **2014**, *60*,
52 810–819.
53
54 (2) Al-Douri, A.; Sengupta, D.; El-Halwagi, M. M. Shale Gas Monetization – A Review of
55 Downstream Processing to Chemicals and Fuels. *J. Nat. Gas Sci. Eng.* **2017**, *45*, 436–455.
56
57
58
59
60

- 1
2
3 (3) Sousa-Aguiar, E. F.; Noronha, F. B.; Faro, A. The Main Catalytic Challenges in GTL
4 (Gas-to-Liquids) Processes. *Catal. Sci. Technol.* **2011**, *1*, 698–713.
- 5
6 (4) Sattler, J. J. H. B.; Ruiz-Martinez, J.; Santillan-Jimenez, E.; Weckhuysen, B. M. Catalytic
7 Dehydrogenation of Light Alkanes on Metals and Metal Oxides. *Chem. Rev.* **2014**, *114*,
8 10613–10653.
- 9
10 (5) Guisnet, M.; Gnep, N. S.; Alario, F. Aromatization of Short Chain Alkanes on Zeolite
11 Catalysts. *Appl. Catal. A, Gen.* **1992**, *89*, 1–30.
- 12
13 (6) Al-Zahrani, S. M. Catalytic Conversion of LPG to High-Value Aromatics: The Current
14 State of the Art and Future Predictions. *Dev. Chem. Eng. Miner. Process.* **2008**, *6*, 101–
15 120.
- 16
17 (7) Guisnet, M.; Gnep, N. S. Aromatization of Propane over GaHMF1 Catalysts. Reaction
18 Scheme, Nature of the Dehydrogenating Species and Mode of Coke Formation. *Catal.*
19 *Today* **1996**, *31*, 275–292.
- 20
21 (8) Price, G. L.; Kanazirev, V. Ga₂O₃/HZSM-5 Propane Aromatization Catalysts: Formation
22 of Active Centers via Solid-State Reaction. *J. Catal.* **1990**, *126*, 267–278.
- 23
24 (9) Meitzner, G. D.; Iglesia, E.; Baumgartner, J. E.; Huang, E. S. The Chemical State of
25 Gallium in Working Alkane Dehydrocyclodimerization Catalysts. In Situ Gallium K-Edge
26 X-Ray Absorption Spectroscopy. *J. Catal.* **1993**, *140*, 209–225.
- 27
28 (10) Biscardi, J. A.; Iglesia, E. Structure and Function of Metal Cations in Light Alkane
29 Reactions Catalyzed by Modified H-ZSM5. *Catal. Today* **1996**, *31*, 207–231.
- 30
31 (11) Anderson, R.F.; Johnson, J.A.; Mowry, J. R. Cyclar: One Step Processing of LPG to
32 Aromatics and Hydrogen. In *Inst. Chem. Eng., Spring National Meeting, Houston, Texas;*
33 *1985.*
- 34
35 (12) Hensen, E. J. M.; Pidko, E. A.; Rane, N.; van Santen, R. A. *Modification of Brønsted*
36 *Acidity of Zeolites by Ga⁺, GaO⁺ and AlO⁺: Comparison for Alkane Activation.* In *Studies*
37 *in Surface Science and Catalysis*; Elsevier B.V.: Beijing, **2007**; Vol. 170, pp 1182–1189.
- 38
39 (13) Faro, C.; Oliveira, V. De. Pulse Reaction Studies of Gallium Modified H-ZSM5 Catalysts
40 with Propane. **2008**, 1155–1158.
- 41
42 (14) De O. Rodrigues, V.; Eon, J. G.; Faro, A. C. Correlations between Dispersion, Acidity,
43 Reducibility, and Propane Aromatization Activity of Gallium Species Supported on
44 HZSM5 Zeolites. *J. Phys. Chem. C* **2010**, *114*, 4557–4567.
- 45
46 (15) Rodrigues, V. D. O.; Faro Júnior, A. C. On Catalyst Activation and Reaction Mechanisms
47 in Propane Aromatization on Ga/HZSM5 Catalysts. *Appl. Catal. A Gen.* **2012**, *435–436*,
48 68–77.
- 49
50 (16) Taha, Z. A.; Deguns, E. W.; Chattopadhyay, S.; Scott, S. L. Formation of Digallium Sites
51 in the Reaction of Trimethylgallium with Silica. *Organometallics* **2006**, *25*, 1891–1899.
- 52
53
54
55
56
57
58
59
60

- 1
2
3 (17) Szeto, K. C.; Gallo, A.; Hernández-Morejudo, S.; Olsbye, U.; De Mallmann, A.; Lefebvre,
4 F.; Gauvin, R. M.; Delevoye, L.; Scott, S. L.; Taoufik, M. Selective Grafting of Ga(i-Bu)₃
5 on the Silanols of Mesoporous H-ZSM-5 by Surface Organometallic Chemistry. *J. Phys.*
6 *Chem. C* **2015**, *119*, 26611–26619.
7
8 (18) Getsoian, A. “Bean”; Das, U.; Camacho-Bunquin, J.; Zhang, G.; Gallagher, J. R.; Hu, B.;
9 Cheah, S.; Schaidle, J. A.; Ruddy, D. A.; Hensley, J. E.; Krause, T. R.; Curtiss, L. A.;
10 Miller, J. T.; Hock, A. S. Organometallic Model Complexes Elucidate the Active Gallium
11 Species in Alkane Dehydrogenation Catalysts Based on Ligand Effects in Ga K-Edge
12 XANES. *Catal. Sci. Technol.* **2016**, *101*, 12–18.
13
14 (19) Cybulskis, V. J.; Pradhan, S. U.; Lovón-Quintana, J. J.; Hock, A. S.; Hu, B.; Zhang, G.;
15 Delgass, W. N.; Ribeiro, F. H.; Miller, J. T. The Nature of the Isolated Gallium Active
16 Center for Propane Dehydrogenation on Ga/SiO₂. *Catal. Letters* **2017**, *147*, 1252–1262.
17
18 (20) Searles, K.; Siddiqi, G. G.; Safonova, O. V.; Coperet, C. Silica-Supported Isolated
19 Gallium Sites as Highly Active, Selective and Stable Propane Dehydrogenation Catalysts.
20 *Chem. Sci.* **2017**, *8*, 2661–2666.
21
22 (21) Kim, W. G.; So, J.; Choi, S. W.; Liu, Y.; Dixit, R. S.; Sievers, C.; Sholl, D. S.; Nair, S.;
23 Jones, C. W. Hierarchical Ga-MFI Catalysts for Propane Dehydrogenation. *Chem. Mater.*
24 **2017**, *29*, 7213–7222.
25
26 (22) Schreiber, M. W.; Plaisance, C. P.; Baumgärtl, M.; Reuter, K.; Jentys, A.; Bermejo-Deval,
27 R.; Lercher, J. A. Lewis-Brønsted Acid Pairs in Ga/H-ZSM-5 to Catalyze
28 Dehydrogenation of Light Alkanes. *J. Am. Chem. Soc.* **2018**, *140*, 4849–4859.
29
30 (23) Bhan, A.; Nicholas Delgass, W. Propane Aromatization over HZSM-5 and Ga/HZSM-5
31 Catalysts. *Catal. Rev.* **2008**, *50*, 19–151.
32
33 (24) Dooley, K. M.; Chang, C.; Price, G. L. Effects of Pretreatments on State of Gallium and
34 Aromatization Activity of Gallium/ZSM-5 Catalysts. *Appl. Catal. A, Gen.* **1992**, *84*, 17–
35 30.
36
37 (25) Dooley, K. M.; Price, G. L.; Kanazirev, V. I.; Hart, V. I. Gallium-Loaded Zeolites for
38 Light Paraffin Aromatization: Evidence for Exchanged Gallium Cation Active Centers.
39 *Catal. Today* **1996**, *31*, 305–315.
40
41 (26) Price, G. L.; Kanazirev, V.; Dooley, K. M.; Hart, V. I. On the Mechanism of Propane
42 Dehydrocyclization over Cation-Containing, Proton-Poor MFI Zeolite. *J. Catal.* **1998**,
43 *173*, 17–27.
44
45 (27) Pidko, E. A.; Kazansky, V. B.; Hensen, E. J. M.; van Santen, R. A. A Comprehensive
46 Density Functional Theory Study of Ethane Dehydrogenation over Reduced Extra-
47 Framework Gallium Species in ZSM-5 Zeolite. *J. Catal.* **2006**, *240*, 73–84.
48
49 (28) Kazansky, V. B.; Subbotina, I. R.; Van Santen, R. A.; Hensen, E. J. M. DRIFTS Study of
50 the Nature and Chemical Reactivity of Gallium Ions in Ga/ZSM-5: II. Oxidation of
51 Reduced Ga Species in ZSM-5 by Nitrous Oxide or Water. *J. Catal.* **2005**, *233*, 351–358.
52
53
54
55
56
57
58
59
60

- 1
2
3 (29) Rane, N.; Overweg, A. R.; Kazansky, V. B.; van Santen, R. A.; Hensen, E. J. M.
4 Characterization and Reactivity of Ga⁺ and GaO⁺ Cations in Zeolite ZSM-5. *J. Catal.*
5 **2006**, *239*, 478–485.
6
7 (30) Hensen, E. J. M.; Pidko, E. A.; Rane, N.; Van Santen, R. A. Water-Promoted
8 Hydrocarbon Activation Catalyzed by Binuclear Gallium Sites in ZSM-5 Zeolite. *Angew.*
9 *Chemie - Int. Ed.* **2007**, *46*, 7273–7276.
10
11 (31) Pidko, E. a.; Hensen, E. J. M.; van Santen, R. A. Self-Organization of Extraframework
12 Cations in Zeolites. *Proc. R. Soc. A Math. Phys. Eng. Sci.* **2012**, *468*, 2070–2086.
13
14 (32) Joshi, Y. V.; Thomson, K. T. The Roles of Gallium Hydride and Brønsted Acidity in
15 Light Alkane Dehydrogenation Mechanisms Using Ga-Exchanged HZSM-5 Catalysts: A
16 DFT Pathway Analysis. *Catal. Today* **2005**, *105*, 106–121.
17
18 (33) Rane, N.; Kersbulck, M.; van Santen, R. A.; Hensen, E. J. M. Cracking of N-Heptane over
19 Brønsted Acid Sites and Lewis Acid Ga Sites in ZSM-5 Zeolite. *Microporous*
20 *Mesoporous Mater.* **2008**, *110*, 279–291.
21
22 (34) Faro, A. C.; Rodrigues, V. D. O.; Eon, J. G. In Situ X-Ray Absorption Study of the
23 Genesis and Nature of the Reduced Gallium Species in Ga/HZSM5 Catalysts. *J. Phys.*
24 *Chem. C* **2011**, *115*, 4749–4756.
25
26 (35) Joshi, Y. V.; Thomson, K. T. High Ethane Dehydrogenation Activity of [GaH]²⁺ Al Pair
27 Sites in Ga/H-[Al]ZSM-5: A DFT Thermochemical Analysis of the Catalytic Sites under
28 Reaction Conditions. *J. Catal.* **2007**, *246*, 249–265.
29
30 (36) Mansoor, E.; Head-Gordon, M.; Bell, A. T. Computational Modeling of the Nature and
31 Role of Ga Species for Light Alkane Dehydrogenation Catalyzed by Ga/H-MFI. *ACS*
32 *Catal.* **2018**, *8*, 6146–6162.
33
34 (37) Schreiber, M. W.; Plaisance, C. P.; Baumgärtl, M.; Reuter, K.; Jentys, A.; Bermejo-Deval,
35 R.; Lercher, J. A. Lewis-Brønsted Acid Pairs in Ga/H-ZSM-5 to Catalyze
36 Dehydrogenation of Light Alkanes. *J. Am. Chem. Soc.* **2018**, *140*, 4849–4859.
37
38 (38) Gonzales, N. O.; Chakraborty, A. K.; Bell, A. T. A Density Functional Theory Study of
39 Hydrogen Recombination and Hydrogen-Deuterium Exchange on Ga/H-ZSM-5. *Top.*
40 *Catal.* **1999**, *9*, 207–213.
41
42 (39) Meriaudeau, P.; Naccache, C. H-ZSM-5 Supported Ga₂O₃ Dehydrocyclisation Catalysts
43 Infrared Spectroscopic Evidence of Gallium Oxide Surface Mobility. *Appl. Catal.* **1991**,
44 *73*, 13–18.
45
46 (40) Joly, J. F.; Ajot, H.; Merlen, E.; Raatz, F.; Alario, F. Parameters Affecting the Dispersion
47 of the Gallium Phase of Gallium H-MFI Aromatization Catalysts. *Appl. Catal. A, Gen.*
48 **1991**, *79*, 249–263.
49
50 (41) Phadke, N.; Van Der Mynsbrugge, J.; Mansoor, E.; Getsoian, A.; Head-Gordon, M.; Bell,
51 A. T. Characterization of Isolated Ga³⁺ Cations in Ga/H-MFI Prepared by Vapor-Phase
52 Exchange of H-MFI with GaCl₃. *ACS Catal.* **2018**, *8*, 6106–6126.
53
54
55
56
57
58
59
60

- 1
2
3 (42) Vannice, Albert, M. *Kinetics of Catalytic Reactions*; Springer US: New York, 2005; pp 1-
4 257.
5
6 (43) Mallikarjun Sharada, S.; Zimmerman, P. M.; Bell, A. T.; Head-Gordon, M. Insights into
7 the Kinetics of Cracking and Dehydrogenation Reactions of Light Alkanes in H-MFI. *J.*
8 *Phys. Chem. C* **2013**, *117*, 12600–12611.
9
10 (44) Zimmerman, P. M.; Head-Gordon, M.; Bell, A. T. Selection and Validation of Charge and
11 Lennard-Jones Parameters for QM/MM Simulations of Hydrocarbon Interactions with
12 Zeolites. *J. Chem. Theory Comput.* **2011**, *7*, 1695–1703.
13
14 (45) Mansoor, E.; Van der Mynsbrugge, J.; Head-Gordon, M.; Bell, A. T. Impact of Long-
15 Range Electrostatic and Dispersive Interactions on Theoretical Predictions of Adsorption
16 and Catalysis in Zeolites. *Catal. Today* **2018**, *312*, 51–65.
17
18 (46) Li, Y.-P.; Gomes, J.; Mallikarjun Sharada, S.; Bell, A. T.; Head-Gordon, M. Improved
19 Force-Field Parameters for QM/MM Simulations of the Energies of Adsorption for
20 Molecules in Zeolites and a Free Rotor Correction to the Rigid Rotor Harmonic Oscillator
21 Model for Adsorption Enthalpies. *J. Phys. Chem. C* **2015**, *119*, 1840–1850.
22
23 (47) Olson, D. H.; Khosrovani, N.; Peters, A. W.; Toby, B. H. Crystal Structure of Dehydrated
24 CsZSM-5 (5.8Å): Evidence for Nonrandom Aluminum Distribution. *J. Phys. Chem. B*
25 **2000**, *104*, 4844–4848.
26
27 (48) Gomes, J.; Zimmerman, P. M.; Head-Gordon, M.; Bell, A. T. Accurate Prediction of
28 Hydrocarbon Interactions with Zeolites Utilizing Improved Exchange-Correlation
29 Functionals and QM/MM Methods: Benchmark Calculations of Adsorption Enthalpies
30 and Application to Ethene Methylation by Methanol. *J. Phys. Chem. C* **2012**, *116*, 15406–
31 15414.
32
33 (49) Shao, Y.; Gan, Z.; Epifanovsky, E.; Gilbert, A. T. B.; Wormit, M.; Kussmann, J.; Lange,
34 A. W.; Behn, A.; Deng, J.; Feng, X.; Ghosh, D.; Goldey, M.; Horn, P. R.; Jacobson, L. D.;
35 Kaliman, I.; Khaliullin, R. Z.; Kuś, T.; Landau, A.; Liu, J.; Proynov, E. I.; Rhee, Y. M.;
36 Richard, R. M.; Rohrdanz, M. A.; Steele, R. P.; Sundstrom, E. J.; Woodcock, H. L.;
37 Zimmerman, P. M.; Zuev, D.; Albrecht, B.; Alguire, E.; Austin, B.; Beran, G. J. O.;
38 Bernard, Y. A.; Berquist, E.; Brandhorst, K.; Bravaya, K. B.; Brown, S. T.; Casanova, D.;
39 Chang, C.-M.; Chen, Y.; Chien, S. H.; Closser, K. D.; Crittenden, D. L.; Diedenhofen, M.;
40 DiStasio, R. A.; Do, H.; Dutoi, A. D.; Edgar, R. G.; Fatehi, S.; Fusti-Molnar, L.; Ghysels,
41 A.; Golubeva-Zadorozhnaya, A.; Gomes, J.; Hanson-Heine, M. W. D.; Harbach, P. H. P.;
42 Hauser, A. W.; Hohenstein, E. G.; Holden, Z. C.; Jagau, T.-C.; Ji, H.; Kaduk, B.;
43 Khistyayev, K.; Kim, J.; Kim, J.; King, R. A.; Klunzinger, P.; Kosenkov, D.; Kowalczyk,
44 T.; Krauter, C. M.; Lao, K. U.; Laurent, A. D.; Lawler, K. V.; Levchenko, S. V.; Lin, C. Y.;
45 Liu, F.; Livshits, E.; Lochan, R. C.; Luenser, A.; Manohar, P.; Manzer, S. F.; Mao, S.-P.;
46 Mardirossian, N.; Marenich, A. V.; Maurer, S. A.; Mayhall, N. J.; Neuscamman, E.; Oana,
47 C. M.; Olivares-Amaya, R.; O'Neill, D. P.; Parkhill, J. A.; Perrine, T. M.; Peverati, R.;
48 Prociuk, A.; Rehn, D. R.; Rosta, E.; Russ, N. J.; Sharada, S. M.; Sharma, S.; Small, D. W.;
49 Sodt, A.; Stein, T.; Stück, D.; Su, Y.-C.; Thom, A. J. W.; Tsuchimochi, T.; Vanovschi, V.;
50 Vogt, L.; Vydrov, O.; Wang, T.; Watson, M. A.; Wenzel, J.; White, A.; Williams, C. F.;
51
52
53
54
55
56
57
58
59
60

- 1
2
3 Yang, J.; Yeganeh, S.; Yost, S. R.; You, Z.-Q.; Zhang, I. Y.; Zhang, X.; Zhao, Y.; Brooks,
4 B. R.; Chan, G. K. L.; Chipman, D. M.; Cramer, C. J.; Goddard, W. A.; Gordon, M. S.;
5 Hehre, W. J.; Klamt, A.; Schaefer, H. F.; Schmidt, M. W.; Sherrill, C. D.; Truhlar, D. G.;
6 Warshel, A.; Xu, X.; Aspuru-Guzik, A.; Baer, R.; Bell, A. T.; Besley, N. A.; Chai, J.-D.;
7 Dreuw, A.; Dunietz, B. D.; Furlani, T. R.; Gwaltney, S. R.; Hsu, C.-P.; Jung, Y.; Kong, J.;
8 Lambrecht, D. S.; Liang, W.; Ochsenfeld, C.; Rassolov, V. A.; Slipchenko, L. V.;
9 Subotnik, J. E.; Van Voorhis, T.; Herbert, J. M.; Krylov, A. I.; Gill, P. M. W.; Head-
10 Gordon, M. Advances in Molecular Quantum Chemistry Contained in the Q-Chem 4
11 Program Package. *Mol. Phys.* **2015**, *113*, 184–215.
12
13
14 (50) Chai, J.-D.; Head-Gordon, M. Long-Range Corrected Hybrid Density Functionals with
15 Damped Atom–atom Dispersion Corrections. *Phys. Chem. Chem. Phys.* **2008**, *10*, 6615-
16 6620.
17
18 (51) Mardirossian, N.; Head-Gordon, M. Thirty Years of Density Functional Theory in
19 Computational Chemistry: An Overview and Extensive Assessment of 200 Density
20 Functionals. *Mol. Phys.* **2017**, *115*, 2315–2372.
21
22 (52) Goerigk, L.; Hansen, A.; Bauer, C. A.; Ehrlich, S.; Najibi, A.; Grimme, S. A Look at the
23 Density Functional Theory Zoo with the Advanced GMTKN55 Database for General
24 Main Group Thermochemistry, Kinetics and Noncovalent Interactions. *Phys. Chem.*
25 *Chem. Phys.* **2017**, *19*, 32184–32215.
26
27 (53) Janda, A.; Vlaisavljevich, B.; Lin, L. C.; Mallikarjun Sharada, S.; Smit, B.; Head-Gordon,
28 M.; Bell, A. T. Adsorption Thermodynamics and Intrinsic Activation Parameters for
29 Monomolecular Cracking of N-Alkanes on Brønsted Acid Sites in Zeolites. *J. Phys.*
30 *Chem. C* **2015**, *119*, 10427–10438.
31
32 (54) Kozuch, S. A Refinement of Everyday Thinking: The Energetic Span Model for Kinetic
33 Assessment of Catalytic Cycles. *Wiley Interdiscip. Rev. Comput. Mol. Sci.* **2012**, *2*, 795–
34 815.
35
36 (55) Kozuch, S.; Shaik, S. How to Conceptualize Catalytic Cycles? The Energetic Span Model.
37 *Acc. Chem. Res.* **2011**, *44*, 101–110.
38
39 (56) Kozuch, S.; Martin, J. M. L. “Turning Over” Definitions in Catalytic Cycles. *ACS Catal.*
40 **2012**, *2*, 2787–2794.
41
42 (57) Kozuch, S.; Shaik, S. A Combined Kinetic-Quantum Mechanical Model for Assessment
43 of Catalytic Cycles: Application to Cross-Coupling and Heck Reactions. *J. Am. Chem.*
44 *Soc.* **2006**, *128*, 3355–3365.
45
46 (58) Janda, A.; Bell, A. T. Effects of Si/Al Ratio on the Distribution of Framework Al and on
47 the Rates of Alkane Monomolecular Cracking and Dehydrogenation in H-MFI. *J. Am.*
48 *Chem. Soc.* **2013**, *135*, 19193–19207.
49
50 (59) Narbeshuber, T. F.; Vinek, H.; Lercher, J. A. Monomolecular Conversion of Light
51 Alkanes over H-ZSM-5. *J. Catal.* **1995**, *157*, 388–395.
52
53
54
55
56
57
58
59
60

- 1
2
3 (60) Gounder, R.; Iglesia, E. Catalytic Consequences of Spatial Constraints and Acid Site
4 Location for Monomolecular Alkane Activation on Zeolites. *J. Am. Chem. Soc.* **2009**, *131*,
5 1958–1971.
6
7 (61) Haag, W. O.; Dessau, R. M.; Lago, R. M. Kinetics and Mechanism of Paraffin Cracking
8 with Zeolite Catalysts. *Stud. Surf. Sci. Catal.* **1991**, *60*, 255–265.
9
10 (62) Kotrel, S.; Knözinger, H.; Gates, B. C. The Haag-Dessau Mechanism of Protolytic
11 Cracking of Alkanes. *Microporous Mesoporous Mater.* **2000**, *35–36*, 11–20.
12
13 (63) Narbeshuber, T. F.; Brait, A.; Seshan, K.; Lercher, J. A. Dehydrogenation of Light
14 Alkanes over Zeolites. *J. Catal.* **1997**, *172*, 127–136.
15
16 (64) Xu, B.; Sievers, C.; Hong, S. B.; Prins, R.; van Bokhoven, J. A. Catalytic Activity of
17 Brønsted Acid Sites in Zeolites: Intrinsic Activity, Rate-Limiting Step, and Influence of
18 the Local Structure of the Acid Sites. *J. Catal.* **2006**, *244*, 163–168.
19
20 (65) Li, W.; Yu, S. Y.; Meitzner, G. D.; Iglesia, E. Structure and Properties of Cobalt-
21 Exchanged H-ZSM5 Catalysts for Dehydrogenation and Dehydrocyclization of Alkanes.
22 *J. Phys. Chem. B* **2001**, *105*, 1176–1184.
23
24 (66) Kolyagin, Y. G.; Ordonsky, V. V.; Khimyak, Y. Z.; Rebrov, A. I.; Fajula, F.; Ivanova, I.
25 I. Initial Stages of Propane Activation over Zn/MFI Catalyst Studied by in Situ NMR and
26 IR Spectroscopic Techniques. *J. Catal.* **2006**, *238*, 122–133.
27
28 (67) Gabrienko, A. A.; Arzumanov, S. S.; Freude, D.; Stepanov, A. G. Propane Aromatization
29 on Zn-Modified Zeolite BEA Studied by Solid-State NMR in Situ. *J. Phys. Chem. C* **2010**,
30 *114*, 12681–12688.
31
32 (68) Gonzales, N. O.; Chakraborty, A. K.; Bell, A. T. A Density Functional Study of the
33 Effects of Metal Cations on the Brønsted Acidity of H-ZSM-5. *Catal. Letters* **1998**, *50*,
34 135–139.
35
36 (69) Vayssilov, G. N.; Rösch, N. Influence of Alkali and Alkaline Earth Cations on the
37 Brønsted Acidity of Zeolites. *J. Phys. Chem. B* **2001**, *105*, 4277–4284.
38
39 (70) Wilkinson, G.; Gillard, R. D.; McCleverty, J. A. *Comprehensive Coordination Chemistry :*
40 *The Synthesis, Reactions, Properties & Applications of Coordination Compounds*;
41 Pergamon Press, 1987; pp 1–1601.
42
43
44
45
46
47
48
49
50
51
52
53
54
55
56
57
58
59
60

Graphical Abstract

